JGR Oceans

RESEARCH ARTICLE
10.1029/2021JC017239

Mechanisms Driving Decadal Changes in the Carbonate System of a Coastal Plain Estuary

Fei Da[1], Marjorie A. M. Friedrichs[1], Pierre St-Laurent[1], Elizabeth H. Shadwick[2], Raymond G. Najjar[3], and Kyle E. Hinson[1]

[1]Virginia Institute of Marine Science, William & Mary, Gloucester Point, VA, USA, [2]CSIRO Oceans and Atmosphere, Hobart, TAS, Australia, [3]Department of Meteorology and Atmospheric Science, The Pennsylvania State University, University Park, PA, USA

Key Points:

- Decadal changes in estuarine surface pH and aragonite saturation state (Ω_{AR}) exhibit large spatial and seasonal variability
- In the upper Chesapeake Bay, changes in riverine alkalinity and dissolved inorganic carbon have increased surface pH in fall and spring
- In the mid- and lower Bay, higher atmospheric CO_2 and reduced nutrient loading have (nearly equally) reduced surface pH and Ω_{AR} in summer

Supporting Information:

Supporting Information may be found in the online version of this article.

Correspondence to:

F. Da,
fda@vims.edu

Citation:

Da, F., Friedrichs, M. A. M., St-Laurent, P., Shadwick, E. H., Najjar, R. G., & Hinson, K. E. (2021). Mechanisms driving decadal changes in the carbonate system of a coastal plain estuary. *Journal of Geophysical Research: Oceans*, *126*, e2021JC017239. https://doi.org/10.1029/2021JC017239

Received 31 JAN 2021
Accepted 3 JUN 2021

Abstract

Understanding decadal changes in the coastal carbonate system is essential for predicting how the health of these waters responds to anthropogenic drivers, such as changing atmospheric conditions and riverine inputs. However, studies that quantify the relative impacts of these drivers are lacking. In this study, the primary drivers of decadal trends in the surface carbonate system, and the spatiotemporal variability in these trends, are identified for a large coastal plain estuary: the Chesapeake Bay. Experiments using a coupled three-dimensional hydrodynamic-biogeochemical model highlight that, over the past three decades, the changes in the surface carbonate system of Chesapeake Bay have strong seasonal and spatial variability. The greatest surface pH and aragonite saturation state (Ω_{AR}) reductions have occurred in the summer in the middle (mesohaline) Bay: −0.24 and −0.9 per 30 years, respectively, with increases in atmospheric CO_2 and reductions in nitrate loading both being primary drivers. Reductions in nitrate loading have a strong seasonal influence on the carbonate system, with the most pronounced decadal decreases in pH and Ω_{AR} occurring during the summer when primary production is strongly dependent on nutrient availability. Increases in riverine total alkalinity and dissolved inorganic carbon have raised surface pH in the upper oligohaline Bay, while other drivers such as atmospheric warming and input of acidified ocean water through the Bay mouth have had comparatively minor impacts on the estuarine carbonate system. This work has significant implications for estuarine ecosystem services, which are typically most sensitive to surface acidification in the spring and summer seasons.

Plain Language Summary

Seawater pH, a measure of how acidic or basic water is, is a crucial water quality parameter influencing the growth and health of marine organisms, such as oysters, fishes and crabs. Decreasing pH, commonly referred to as acidification, is a severe environmental issue that has been exacerbated by human activities since the industrial revolution. In the open ocean, elevated atmospheric carbon dioxide is the key driver of acidification. However, in coastal environments the drivers are particularly complex due to changing human influences on land. In this study the primary drivers of acidification in the Chesapeake Bay over the past three decades are identified via the application of a three-dimensional ecosystem model. Increased atmospheric CO_2 concentrations and decreased terrestrial nutrient inputs are two primary drivers causing nearly equal reductions in pH in surface waters of the Bay. The pH reductions resulting from decreased nutrient loads indicate that the system is reverting back to more natural conditions when human-induced nutrient inputs to the Bay were lower. As nutrient reduction efforts to improve coastal water quality continue in the future, controlling the emissions of anthropogenic CO_2 globally becomes increasingly important for the shellfish industry and the ecosystem services it provides.

1. Introduction

Global atmospheric CO_2 concentrations have increased from 320 ppm in the 1960s to a present-day value of 410 ppm due to anthropogenic activities (Keeling & Keeling, 2017). This increase has resulted in significant warming in the atmosphere and the global ocean (Hartmann et al., 2013; Johnson & Lyman, 2020), and significant reductions in open ocean pH and aragonite saturation state (Ω_{AR}) at mean rates of −0.02 pH units decade^{-1} and 0.08 decade^{-1}, respectively, over the past three decades (Doney et al., 2009; Takahashi et al., 2014). These changes, along with other human-driven environmental alterations, will likely impact marine ecosystem services, such as fisheries and aquaculture (Doney, et al., 2020).

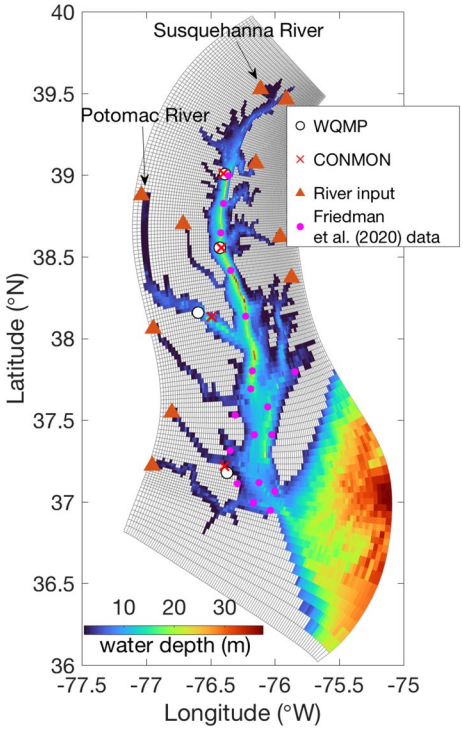

Figure 1. The horizontal grid and bathymetry of ChesROMS-ECB. Symbols denote stations with recent carbonate system data (Friedman et al., 2020), Continuous Monitoring (CONMON) data, and nearby Water Quality Monitoring Program (WQMP) stations used for comparison in Table 3. From north to south, WQMP stations include CB3.3 W, CB4.3 C, LE2.2 and WE4.3; CONMON stations include Sandy Point South Beach, Gooses Reef, St. Georges Creek, and Goodwin Islands. Fluxes from the watershed are aggregated into 10 points (orange triangles) corresponding to the location of the largest rivers.

In coastal ecosystems, local changes in nutrient inputs from the watershed have crucial impacts on the carbonate system and can alter pH and Ω_{AR} via production and consumption of total alkalinity (TA) and dissolved inorganic carbon (DIC). Specifically, enhanced algal growth from increased nitrogen loads (e.g., eutrophication) provides excess organic material for aerobic decomposition, particularly in warmer seasons, which lowers the pH and Ω_{AR} in subsurface and/or downstream coastal waters (Borges & Gypens, 2010; Cai et al., 2011; Cai, Feely, et al., 2020; Feely et al., 2010; Rheuban et al., 2019; Sunda & Cai, 2012; Zhao et al., 2020). Furthermore, recent human activities (e.g., reduced mining and more agricultural usage of lime) have been found to increase riverine TA fluxes in some large rivers in the United States (US) (Kaushal et al., 2013; Raymond & Oh, 2009; Stets et al., 2014), which potentially may offset some of the pH and Ω_{AR} reductions due to increased atmospheric CO_2 and eutrophication.

Previous studies have focused on the physiological stress that the reduction of pH in coastal waters (defined here as "coastal acidification") causes for marine calcifying organisms. Low pH and low Ω_{AR} can affect physiological processes of bivalves, including respiration rate, hatching success, shell growth, and feeding (Waldbusser & Salisbury, 2014; Waldbusser et al., 2015). The coastal shellfish industry is at considerable risk from increasing impacts of these reductions in pH and Ω_{AR} (Ekstrom et al., 2015), as well as other stressors, including hypoxia (Gobler et al., 2014; Gobler & Baumann, 2016; Tomasetti & Gobler, 2020); thus, for future coastal conservation and management efforts, it is crucial to further our understanding of the roles anthropogenic drivers play in causing long-term changes in the carbonate system.

The Chesapeake Bay, a large and productive coastal plain estuary in the US (Figure 1), has a shellfish industry that has been impacted over the past century by local watershed inputs related to various anthropogenic activities. In the 1960s and 1970s, nutrient loading to the Chesapeake Bay increased rapidly due to the expansion of industry and urbanization, as well as increases in agricultural usage of fertilizer (Yang et al., 2015; Pan et al., 2021), resulting in excess algal blooms, eutrophication, and severe summer hypoxia (Hagy et al., 2004; Nixon, 1995; Seliger et al., 1985). More recently, nutrient management efforts aiming to control hypoxia have led to reductions in nitrate (NO_3^-) and organic nitrogen inputs to the Chesapeake Bay (Harding et al., 2016; Moyer & Blomquist, 2020; Zhang et al., 2015). Continuous management actions required by Chesapeake Bay Total Maximum Daily Load (TMDL; USEPA, 2010) regulations are expected to further reduce nutrient inputs (Irby & Friedrichs, 2019). In addition, TA increases in rivers draining the Chesapeake Bay watershed have resulted from decreased acid mine drainage (Kaushal et al, 2013; Raymond & Oh, 2009; Stets et al., 2014). DIC concentrations have increased as well, due not only to decreased acid mine drainage, but also agricultural liming, concrete weathering and acid deposition (Raymond & Hamilton, 2018). The relative ratio between the increase in riverine TA and DIC has likely impacted the net carbonate buffering capacity of tributaries in the Chesapeake Bay watershed.

While several recent studies have focused on the spatial and seasonal variability of the Chesapeake Bay carbonate system (Brodeur et al., 2019; Chen et al., 2020; Friedman et al., 2020; Shadwick, Friedrichs, et al., 2019; Shen et al., 2019), research on long-term change is relatively rare. Waldbusser et al. (2011) conducted linear regressions of glass electrode pH data (1985–2008). Although they found significant decreasing trends in surface pH in the lower Bay, the changes in pH sampling methodology prior/after 1996 (Herrmann et al., 2020) likely bias the trends calculated using these data. Herrmann et al. (2020) excluded these early pH data in the Chesapeake Bay and analyzed the spatiotemporal patterns of the calculated CO_2 partial pressure (pCO_2) and air-water CO_2 exchange over the years 1998–2018. The Bay was found to be a weak source of CO_2 to the atmosphere, with more outgassing during the early part of the record, perhaps in

response to lower streamflow and greater net heterotrophy during that time. Najjar et al. (2020) identified TA increases over many decades in tidal tributaries of the Chesapeake Bay, including the upper main stem Bay, which reflected a combination of increasing riverine TA and, in the Potomac River Estuary, a declining TA sink.

Several recent modeling studies have also advanced our current understanding of long-term changes in the Chesapeake Bay carbonate system. St-Laurent et al. (2020) showed that local changes in nitrogen loading and global changes in atmospheric CO_2 have been the two primary drivers of change in the Chesapeake Bay inorganic carbon budget over the past century. Specifically, both drivers brought the Bay closer to being a net sink of atmospheric CO_2 by roughly the same amount (~30 Gg C y^{-1}). Using a similar coupled biogeochemical-circulation model, Shen et al. (2020) examined spring and summer changes over the past 30 years and found that increased atmospheric CO_2 and nutrient loading played key roles in impacting Chesapeake Bay surface pH and Ω_{AR}. Shen et al. (2020) also found that alkalinization of the Susquehanna River has simultaneously increased pH in the upper Bay. Although these earlier studies form a solid basis for a general understanding of long-term change in the Bay, they do not focus on how these changes vary seasonally. Given that the Bay is warming three to four times faster in the warmer months of the year compared to the cooler months (Hinson et al., 2021), it is possible that long-term trends in the carbonate system are also undergoing more significant trends in the summer season. In addition, several other drivers need to be explicitly evaluated to delineate the impacts of various physical and biogeochemical processes on the carbonate system. For example, impacts of drivers such as increasing downward long-wave radiation (Hinson et al., 2021), increasing DIC concentrations along the Mid-Atlantic Bight (MAB; Xu et al., 2020) and decreasing organic nutrient inputs have not previously been examined.

To address this knowledge gap, this study combines water quality data and numerical model simulations to assess the relative impacts of both global- and local-scale drivers on the mainstem Chesapeake Bay surface carbonate system over the past three decades. The impacts of each individual driver, and all six drivers combined, are analyzed over the complete seasonal cycle. Given that most calcifying organisms reside in shallow shoals and tributaries where water tends to be more well-mixed, this study focuses on the decadal changes in Chesapeake Bay surface waters. Datasets and numerical modeling tools are described in Section 2. In Section 3 the results of the long-term data analyses and model sensitivity experiments are presented. Relative seasonal and spatial impacts of these drivers on the Bay carbonate system are discussed in Section 4, and implications of this work are summarized in Section 5.

2. Methods

2.1. Carbonate System Data in the Chesapeake Bay

A plethora of long-term water quality cruise data, as well as high-frequency buoy data and short-term carbonate system data from shipboard sampling are available throughout the Chesapeake Bay. The Chesapeake Bay Water Quality Monitoring Program (WQMP) has been thoroughly monitoring physical and biogeochemical fields at more than 100 Chesapeake Bay stations since 1984 (Chesapeake Bay Program, 2012; Olson et al., 2012). Glass electrode pH is generally measured once each month from October to March, and twice each month from April to September at these stations. This study restricts data analysis to 1996–2018 because quality control of the WQMP pH data revealed unrealistically high pH in Virginia stations prior to 1996 (Herrmann et al., 2020). Additionally, high frequency (15-min interval) electrode pH data are available since the mid-2000s at four Continuous Monitoring (CONMON; CBNERR-VA VIMS, 2020) stations in close proximity to WQMP mainstem stations (Figure 1). The electrode pH measurements from both datasets have a precision of ±0.2 pH units or better.

Discrete samples for measurements of DIC and TA were collected at 18 main stem stations (Figure 1) on 14 WQMP cruises between June 2016 and June 2018 (Friedman et al., 2020; Shadwick, De Meo, & Friedman, 2019). Samples were collected in borosilicate bottles one meter below the surface and one meter above the bottom, as well as at two intermediate depths above and below the pycnocline. In total, 552 pairs of DIC and TA measurements were made, along with corresponding measurements of temperature, salinity, and oxygen. Sample analyses followed procedures as described in Dickson et al. (2007), with an accuracy on the order of ±2 and ± 3 μmol kg^{-1} for DIC and TA measurements, respectively. Following analysis, pH, pCO_2

and Ω_{AR} were computed in CO2SYS (van Heuven et al., 2011) using the equilibrium constants of Cai and Wang (1998), which have been found to be more appropriate for low-salinity estuarine waters (Dinauer & Mucci, 2017; Herrmann et al., 2020).

2.2. Estuarine Carbon Biogeochemistry Model: ChesROMS-ECB

This study used a coupled three-dimensional hydrodynamic-carbon-biogeochemistry model (ChesROMS-ECB) to quantify the relative impacts of multiple global and local drivers on the Chesapeake Bay carbonate system. The ChesROMS-ECB model uses physical components from version 3.6 of the Rutgers branch of the Regional Ocean Modeling System (ROMS, Shchepetkin & McWilliams, 2005). The resolution of the horizontal orthogonal curvilinear grid (Xu et al., 2012) ranges from 430 m to ∼2 km inside the Chesapeake Bay, with lower resolution (up to ∼10 km) along the southern end of the open boundary in the MAB (Figure 1). The model, which includes 20 stretched terrain-following vertical levels, has been evaluated extensively with physical and biogeochemical observations in previous studies pertaining to Chesapeake Bay oxygen, nitrogen and carbon dynamics (Da et al., 2018; Feng et al., 2015; Irby et al., 2018; Kim et al., 2020; Moriarty et al., 2021; St-Laurent et al., 2020; Turner et al., 2021).

The primary focus of this work is the carbon module, which is based on the implementation of St-Laurent et al. (2020; see that paper's supplementary material for the full equations). The carbon module consists of the following inorganic and organic state variables: DIC, TA, small and large detritus of carbon, and both semilabile and refractory dissolved organic carbon. Phytoplankton and zooplankton carbon is assumed to be equivalent to their nitrogen counterparts in a constant Redfield ratio. Compared to the previous model implementation (St-Laurent et al., 2020), this version of ChesROMS-ECB accounts for the total impact of NH_4^+ and NO_3^- on TA by linking all related sink and source terms following Wolf-Gladrow et al. (2007), their Section 5.3; corresponding to organic matter remineralization, phytoplankton and zooplankton metabolism, nitrification, denitrification and sediment flux in ChesROMS-ECB). The carbon module calculates pCO_2 from modeled DIC, TA, temperature and salinity using carbonic acid equilibrium constants of Cai and Wang (1998). These constants are also used to compute pH and Ω_{AR} diagnostically from the modeled variables using CO2SYS. In addition, our gas transfer velocity parameterization is updated from Wanninkhof (1992) to Wanninkhof (2014), which gives a slightly smaller gas transfer velocity.

There are several assumptions made in the model regarding the carbonate system. First, biological terms have no limitations that depend on pH or pCO_2. Secondly, due to the lack of observations required for developing model parameterizations suitable for the time and space scales analyzed here, the biogeochemical module does not include calcium carbonate cycling. Finally, Herrmann et al (2020) estimated that organic alkalinity concentration in the Chesapeake Bay has a mean of 20 meq m^{-3} and standard deviation of 30 meq m^{-3}, which are both much smaller than typical TA concentrations throughout the main stem Bay (600–2,200 meq m^{-3}; Najjar et al., 2020). Therefore, organic alkalinity is assumed to be insignificant in this study.

2.3. Model Forcing

Atmospheric forcing for ChesROMS-ECB is derived from ERA5 (Copernicus Climate Change Service, 2017), an atmospheric reanalysis product providing global atmospheric conditions from 1979 to the present. Three-hourly surface atmospheric fields with a horizontal resolution of 0.25° (winds, downward long-wave radiation, net short-wave radiation, precipitation, dewpoint temperature, air temperature and pressure) are obtained from ERA5 and interpolated to a 0.2° grid to create atmospheric forcing files for ChesROMS-ECB between 1979 and 2019. The ERA5 forcing was found to better represent interannual atmospheric temperature variability and long-term trends in the Chesapeake Bay region (Hinson et al., 2021) compared to earlier studies (Feng et al., 2015) using the North American Regional Reanalysis (Mesinger et al., 2006).

The riverine nitrogen, carbon and sediment loadings used in this study are derived from the Phase 6 Chesapeake Bay Watershed Model (CBPWM; Chesapeake Bay Program, 2017) and United States Geological Survey (USGS) data. For the period 1985–2014, daily estimates of freshwater discharge, temperature, NO_3^-, NH_4^+, organic nitrogen and sediment concentrations from the CBPWM are used as river inputs for ChesROMS-ECB. For the most recent years when CBPWM results are unavailable (2015–2019), climatological CBPWM sediment and organic nitrogen concentrations and USGS WRTDS (Weighted Regression on

Time, Discharge, and Season) NO_3^- concentrations (Moyer & Blomquist, 2020) are combined with USGS discharge (Bever et al., 2021). Riverine organic carbon concentrations are derived from the CBPWM organic nitrogen concentrations and fixed carbon-to-nitrogen ratios from Hopkinson et al. (1998). Specifically, dissolved and particulate detrital carbon-to-nitrogen ratios are set to 10:1 and 106:16, respectively. Daily concentrations of USGS riverine TA and calculated estimates of DIC (see Najjar et al., 2020 for details) are directly prescribed as model inputs to the Susquehanna and the Potomac Rivers. In recent years when USGS products are not available, TA and DIC concentrations are computed from river discharge and the corresponding discharge-TA and discharge-DIC relationships (Figure S1) derived from long-term daily USGS data products. Riverine TA and DIC concentrations in other smaller tributaries are held constant in time, following St-Laurent et al. (2020). These concentrations of organic carbon, TA, and DIC are combined with the freshwater discharge from the CBPWM (1985–2014) and the USGS (2015–2019) to provide riverine carbon and TA fluxes to ChesROMS-ECB.

Temperature and salinity along the model open boundary are derived from the World Ocean Database version 2018 (WOD 2018). Profiles (Boyer et al., 2018) within 10 km of the open boundary over the years 2008–2018 are used to create a monthly climatology, which represents the reference boundary conditions for the year 2013. A two-dimensional spatial interpolation is first conducted on the temperature and salinity profiles to obtain monthly climatologies for the nine months when data are available. A one-dimensional temporal interpolation is then applied to these monthly climatologies to obtain a complete seasonal cycle of spatially varying temperature and salinity climatology for the reference year 2013. Long-term trends of these two variables are extracted from the same WOD data set over the years 1985–2018. Specifically, linear regressions are applied to depth-averaged temperature and salinity to calculate the monthly long-term trends, which are then superimposed onto the monthly climatologies (of year 2013) to create interannually varying temperature and salinity boundary conditions from 1985 to 2018. Saturated O_2 concentrations along the outer boundary are calculated from these temperature and salinity fields using a solubility equation (Garcia & Gordon, 1992). The MAB TA-salinity relationship from Cai et al. (2010) is applied to obtain oceanic TA concentrations. Long-term TA and DIC values spanning a latitudinal interval from 36° to 38°N (Xu et al., 2020) are used to calculate monthly TA-to-DIC ratios near the model boundary in the MAB. These ratios from 2011 to 2015 are averaged to estimate the spatially invariant reference ratio for the year 2013. The rate of change in TA-to-DIC ratios from 1982 to 2015 is calculated via a linear regression method: $TA/DIC = -3.47 \times 10^{-5}{}_t + 1.099$, $N = 408$, $p < 0.001$, where t is the time in months ($t = 0$ refers to January 1982) and N is the number of monthly data points. This rate is superimposed onto the reference ratio in 2013 to generate a time series of TA-to-DIC ratio that decreases with time. DIC concentrations on the open boundary in the MAB are computed as TA concentrations divided by the TA-to-DIC ratio.

2.4. Model Experiments

Two five-year reference runs and seven sensitivity experiments are conducted in this study. The first reference run is conducted from 1985 to 1989 (Ref_{1985}) for comparisons against sensitivity simulations, as these are the earliest years for which WQMP data are available; the second reference run is conducted from 2015 to 2019 (Ref_{2015}) for model evaluation using recent carbonate system data (Friedman et al., 2020). Seven sensitivity experiments are compared to the reference run Ref_{1985} to quantify the relative impacts of global- and local-scale drivers on the decadal trends of the Chesapeake Bay carbonate system (Table 1). These sensitivity experiments have the same model forcings as in Ref_{1985}, except that one of the following is individually modified to represent the conditions 30 years later (2015–2019): (1) increased atmospheric CO_2 concentrations ($AtmCO_2$), (2) increased atmospheric temperature and downwelling long-wave radiation (AtmT), (3) increased oceanic DIC concentrations (OcnC), (4) decreased riverine NO_3^- concentrations and the related increase in riverine TA concentrations ($RivNO_3$), (5) decreased riverine organic nitrogen concentrations (RivON), and (6) increased riverine TA and DIC concentrations (RivC). In a final experiment (7) all of these global and local forcings are changed simultaneously (All, Table 1). Freshwater discharge in each sensitivity experiment was the same as in the Ref_{1985} simulation. The increases in riverine TA due to reduced riverine NO_3^- concentrations are excluded from the RivC experiment, since these increases are included in the $RivNO_3$ scenario.

Table 1
The Nine Numerical Experiments Conducted in This Study

Simulation	Atmospheric CO_2	Atmospheric thermal forcing	Riverine NO_3^-	Riverine organic N	Riverine DIC & TA	Oceanic DIC
Ref_{1985}	1985–1989	1985–1989	1985–1989	1985–1989	1985–1989	1985–1989
Ref_{2015}	2015–2019	2015–2019	2015–2019	2015–2019	2015–2019	2015–2019
$AtmCO_2$	**Ref_{1985} + Δ↑[a] in atmos. CO_2**	1985–1989	1985–1989	1985–1989	1985–1989	1985–1989
AtmT	1985–1989	**Ref_{1985} + Δ↑ in atmos. forcing**	1985–1989	1985–1989	1985–1989	1985–1989
$RivNO_3$	1985–1989	1985–1989	**Ref_{1985} + Δ↓[b] in riv. NO_3^-**	1985–1989	**Ref_{1985} + Δ↑ in riv. TA_{NO3}[c]**	1985–1989
RivON	1985–1989	1985–1989	1985–1989	**Ref_{1985} + Δ↓ in riv. organic N**	1985–1989	1985–1989
RivC	1985–1989	1985–1989	1985–1989	1985–1989	**Ref_{1985} + Δ↑ in riv. DIC & TA_C[d]**	1985–1989
OcnC	1985–1989	1985–1989	1985–1989	1985–1989	1985–1989	**Ref_{1985} + Δ↑ in ocn. DIC**
All	**Ref_{1985} + Δ↑ in atmos. CO_2**	**Ref_{1985} + Δ↑ in atmos. forcing**	**Ref_{1985} + Δ↓ in riv. NO_3^-**	**Ref_{1985} + Δ↓ in riv. organic N**	**Ref_{1985} + Δ↑ in riv. DIC & TA**	**Ref_{1985} + Δ↑ in ocn. DIC**

[a]Δ↑ refers to 30-year increase in model forcings (Section 2.4). [b]Δ↓ refers to 30-year decrease in model forcings. [c]Δ↑ in riv. TA_{NO3} refers to the increase in total alkalinity due to reduced riverine NO_3^- concentrations. Carbonate alkalinity in $RivNO_3$ experiment remains the same as in the 1985–1989 reference run (Ref_{1985}). [d]Δ↑ in riv. TA_C refers to the increase in carbonate alkalinity, since the increase in alkalinity due to reduced riverine NO_3^-concentrations is included in the $RivNO_3$ experiment.

Note. Riverine and oceanic inputs are modified by only changing concentrations, while freshwater discharge remains the same as in the Ref_{1985} simulation.

For the sensitivity experiments, linear regression is used to calculate the long-term change (2015–2019 relative to 1985–1989) in atmospheric forcing conditions, as well as biogeochemical concentrations in the rivers and on the continental shelf. Seasonality is considered in the change, where applicable. Specifically, for the sensitivity experiment $AtmCO_2$, annual mean atmospheric CO_2 records at Mauna Loa (Keeling & Keeling, 2017) are used to estimate a 57 ppm increase in CO_2 concentrations over this 30-year time period (independent of season). ERA5 atmospheric temperature and downwelling long-wave radiation have been generally increasing (0.7°C and 6.3 W m^{-2} per 30 years, respectively), but with substantially greater warming occurring from spring to early fall (Hinson et al., 2021). Thus, seasonally varying changes in atmospheric temperature and long-wave radiation are applied to the sensitivity experiment AtmT (Figure 2a). Atmospheric variables other than temperature and downwelling long-wave radiation exhibit minor changes over the 30-year period of interest and thus are left unmodified. Oceanic DIC concentrations along the model boundary in the OcnC experiment are increased via a reduced TA-to-DIC ratio (see Section 2.3), resulting in a 23 mmol m^{-3} increase in boundary DIC concentrations over these 30 years. For the $RivNO_3$, RivON, and RivC sensitivity experiments, seasonally varying 30-year changes in terrestrial inputs (riverine NO_3^-, organic nitrogen, TA and DIC) are applied to the largest two tributaries of the Bay (the Susquehanna and Potomac Rivers) since these trends vary substantially between seasons (Figures 2b and 2c). Specifically, monthly trends are computed via linear regression of USGS WRTDS flow-normalized riverine NO_3^- and organic nitrogen concentrations and USGS TA and calculated DIC products. On average, the 30-year changes in Susquehanna NO_3^-, organic nitrogen, TA, and DIC concentrations are −20 mmol m^{-3}, –12 mmol m^{-3}, +195 meq m^{-3}, and +146 mmol m^{-3}, respectively (see Section 1). The increase in TA is thus dominated by the increase in carbonate alkalinity, while NO_3^- reduction only accounts for one tenth of the total increase. The increase in TA is also proportionally larger than the increase in DIC in the Susquehanna River (Figure 2c). Although total organic carbon loading has increased over the past three decades (Zhang & Blomquist, 2018), there are no significant trends in flow-normalized concentrations (Zhang, pers. comm.). Additionally, in order to isolate the impact of long-term trends in nutrient inputs on the carbonate system without perturbing the estuarine physics, only the nitrogen concentrations are modified in this study (i.e., freshwater discharge and organic carbon concentrations are unchanged in sensitivity simulations). Model

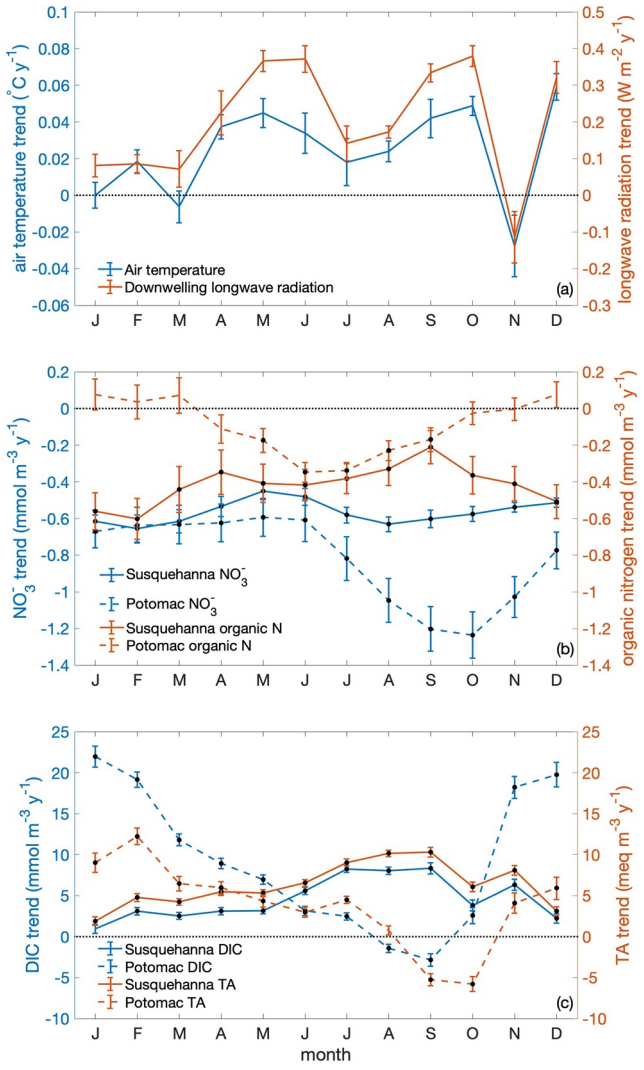

Figure 2. Seasonality of decadal trends applied to model sensitivity experiments for: (a) atmospheric temperature and downwelling long-wave radiation, (b) riverine NO_3^- and organic nitrogen concentrations, and (c) riverine total alkalinity and dissolved inorganic carbon concentrations. The whiskers in panel (a) are one standard deviation, representing the spatial variability of monthly trends, and the whiskers in panel (b) and (c) represent the standard error of the slope of the monthly linear regression. Black dots in panel (b) and (c) indicate significant linear trends ($p < 0.05$).

results from each of the seven sensitivity experiments are compared to the outputs from Ref_{1985} to quantify the contribution of each driver to the total carbonate system variability over the past 30 years (Table 1). The sum of these individual changes is computed and compared with the difference between Ref_{1985} and All simulation in which all global and local forcings are changed simultaneously.

2.5. Model Skill Assessment and Decadal Trend Calculation

Model skill was assessed by comparing model results from Ref_{2015} to observations along the main stem of the Chesapeake Bay. Since modeled temperature and salinity have been extensively evaluated with WQMP data as shown in Feng et al. (2015) and Hinson et al. (2021) and nitrogen concentrations have been evaluated in Da et al. (2018), this study focuses on the evaluation of the carbonate system. Because of the large uncertainties associated with electrode pH data from the WQMP, recent carbonate system data from the 18 main stem stations (Figure 1) from Friedman et al. (2020) are used here for model evaluation. Specifically, hourly modeled carbonate system variables matching the specific times when data were collected are selected for point-to-point comparisons throughout the water column. Model skill statistics include root-mean squared difference (RMSD) and model bias; normalized metrics are visualized on a target diagram (Hofmann et al., 2008; Jolliff et al., 2009) in the online supplementary material. All pH observations from Friedman et al. (2020) and model results are reported on the total scale. Additional model skill statistics for years 1985–1989 are included in the online supplementary material (Table S1).

Long-term linear trends in surface pH are also computed from the glass electrode WQMP data (1996–2018) and CONMON data (mid-2000s to present, see Section 2.1) in each month of the year. These pH data are reported on the NBS scale. The linear regressions are conducted over all years that are available in each data set. Trends calculated from the two different sources of glass electrode pH data are compared to the modeled changes in the carbonate system caused by all drivers combined (sensitivity experiment All in Section 2.4). An alternative method would be to derive the 30-year changes in the carbonate system as the difference between our two reference simulations (Ref_{2015} – Ref_{1985}). However, the large interannual variability in terrestrial and atmospheric inputs results in large perturbations in the Chesapeake Bay carbonate system from year to year, which could bias the 30-year changes due to specific wet and dry conditions (e.g., high precipitation and discharge in 2018). The difference between the reference run (Ref_{1985}) and the All sensitivity experiment is thus a more robust method for estimating the decadal trends.

3. Results

3.1. Evaluation of Modeled Carbonate System

Point-to-point comparisons with observations show that the model reproduces temperature, salinity, oxygen, TA, and DIC quite well throughout the Bay (Table 2; Figure S2), but some discrepancies exist in pH and Ω_{AR}, particularly in low-salinity regions (Figure 3). As described in Section 2, observed and modeled pH (total scale) and Ω_{AR} are calculated in CO2SYS using the equilibrium constants of Cai and Wang (1998). Skill metrics of temperature and salinity (Table 2) show small model bias (0.04°C and −0.56 units, respectively) and RMSD (~1°C and ~2 units). TA and DIC concentrations in the Bay range from 900 to 2200 meq

Table 2
Summary of Model Skill Metrics Calculated for Physical and Biogeochemical Fields Throughout the Water Column (N^a = 552)

Variable	Mean ± standard deviation		Bias	Unbiased RMSD[b]	RMSD
	Model	Observation			
Temperature (°C)	18.42 ± 7.69	18.38 ± 7.97	0.04	1.09	1.09
Salinity	18.19 ± 5.53	18.75 ± 4.96	−0.56	1.94	2.02
TA (meq m^{-3})	1723 ± 222	1718 ± 203	5.41	89.97	90.02
DIC (mmol m^{-3})	1599 ± 221	1621 ± 197	−22.23	105.89	108.08
pH (total)	8.06 ± 0.31	7.97 ± 0.25	0.09	0.22	0.24
Ω_{AR}	1.67 ± 0.82	1.34 ± 0.53	0.33	0.59	0.68
Oxygen (mg L^{-1})	8.04 ± 2.65	7.89 ± 2.71	0.15	1.24	1.25

[a]*N* is the total number of data points collected from June 2016 to June 2018. [b]RMSD refers to root-mean squared difference. Unbiased RMSD represents the RMSD after removing the mean from the model estimates or observations (Jolliff et al., 2009).

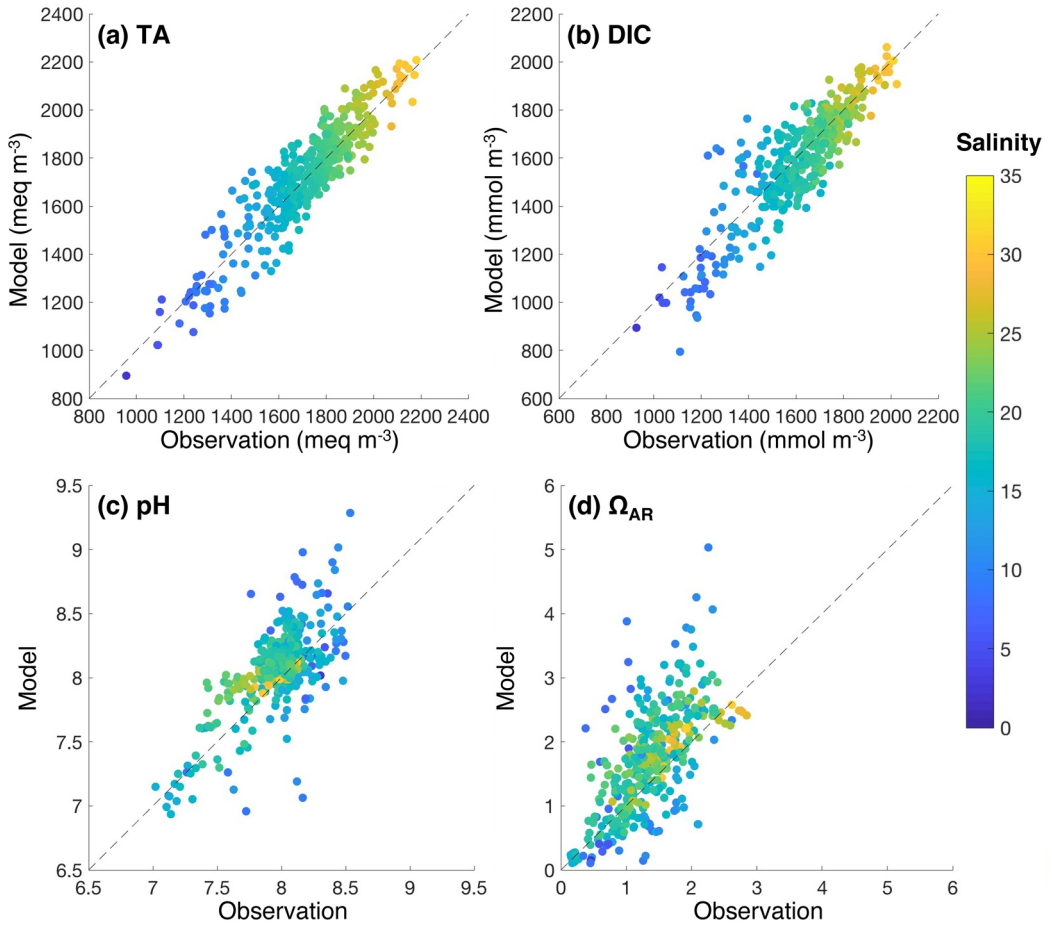

Figure 3. Model-data comparisons as a function of salinity for: (a) total alkalinity, (b) dissolved inorganic carbon, (c) pH (total scale) and (d) Ω_{AR} using recent carbonate system data (Friedman et al., 2020) throughout the water column at 18 stations (see Figure 1) from 2016 to 2018.

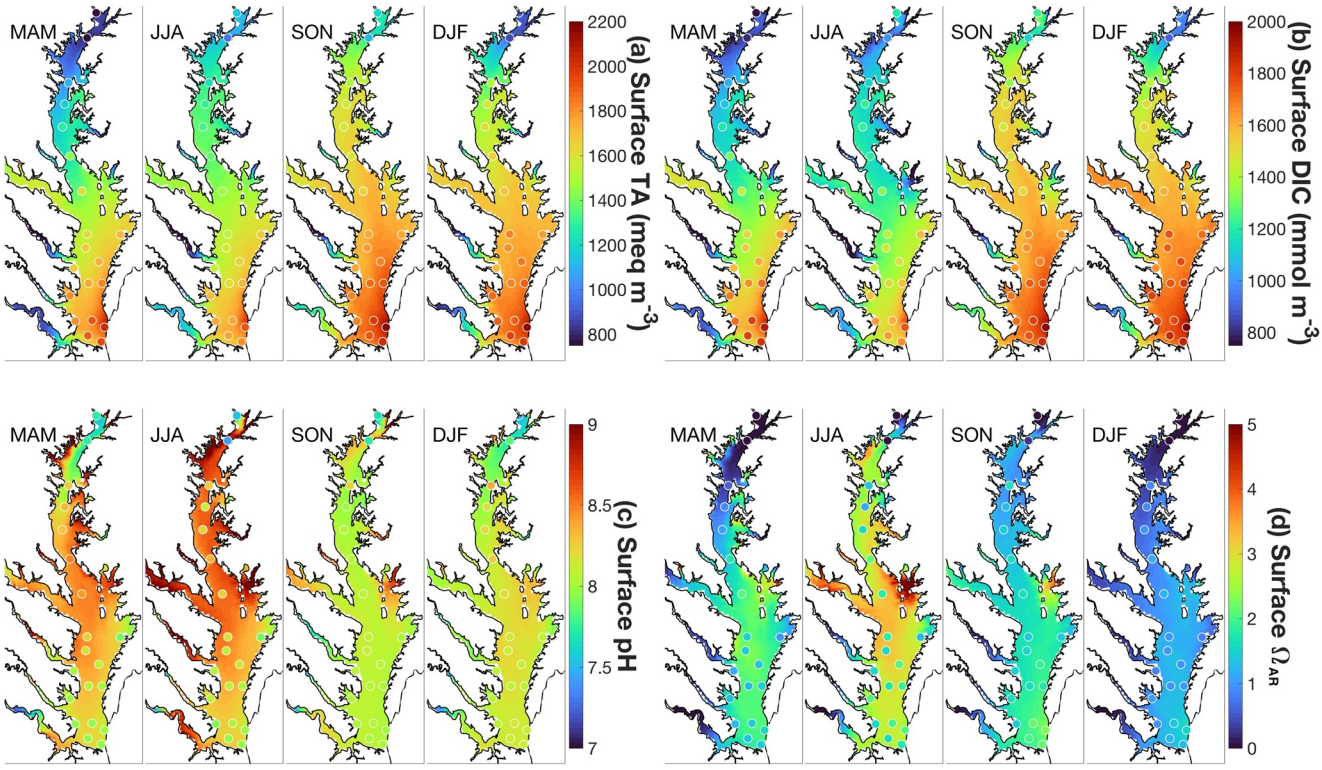

Figure 4. Comparison between model and observations for surface (a) total alkalinity, (b) dissolved inorganic carbon, (c) pH (total scale) and (d) Ω_{AR}. The colored contours represent seasonally averaged model results for June 2016 to June 2018; the circles represent recent point observations from Friedman et al. (2020) made over the same time period. (MAM = spring, JJA = summer, SON = fall, and DJF = winter).

m^{-3} and 900–2100 mmol m^{-3}, respectively, with the lowest values in the upper Bay (salinity ≤ 5, more than 250 km from the Bay mouth) and the highest values in the lower Bay (salinity > 20, less than 75 km from the Bay mouth). The model captures the observed TA and DIC concentrations relatively well (R^2 = 0.84 and 0.77, respectively; N = 552, Figures 3a and 3b), while the pH and Ω_{AR} comparisons are not quite as good especially in the upper Bay (R^2 = 0.50 and 0.48, respectively; N = 552, Figures 3c and 3d). On average, the model overestimates TA by ~5 meq m^{-3} and underestimates DIC by ~22 mmol m^{-3} (Table 2), resulting in a positive bias in model estimates of pH and Ω_{AR} (0.09 pH units and 0.33, respectively). A closer examination of the modeled pH and Ω_{AR} shows that discrepancies are largest in relatively fresh regions in the summer when primary production is the highest. It is likely that an overestimation of primary production in recent wet years causes the overestimation of summer pH and Ω_{AR}, which is consistent with the positive bias in modeled oxygen concentrations at the surface (0.33 mg L^{-1}). Additional calculations suggest that these biases in pH and Ω_{AR} have minimal impacts on the decadal trends computed in this study (Figure S3).

Seasonal averages of modeled fields in surface waters are compared to the mean observations, which shows that the spatial and temporal variability in the carbonate system is captured relatively well by the model, although some spatiotemporal bias exists (Figure 4). Observed TA and DIC concentrations (Figures 4a and 4b) both increase from their minimum values in the relatively fresh tributaries (~900–1,200 meq m^{-3} and mmol m^{-3}) to their maximum values in the south (~1,800–2100 meq m^{-3} and ~1,600–1,900 mmol m^{-3}) where the Bay connects to the Atlantic Ocean. Seasonally, TA and DIC concentrations are generally lower in the spring and summer, and are higher in the fall and winter. This spatial and seasonal variability in TA and DIC is well simulated in the model, excluding underestimates in the lower Bay during the spring, which are consistent with a slight overestimation of primary productivity in this region (St-Laurent et al., 2020). Maximum pH values (Figure 4c) are observed in the middle Bay, specifically in the spring and summer, where and when primary production is usually highest. Overall, the model captures the seasonal variability in pH relatively well, except in the summer when pH is overestimated. Similar to pH, surface Ω_{AR} (Figure 4d) is lowest in the upper Bay and tributaries, and is higher in the middle and lower Bay. Modeled Ω_{AR} reproduces

Table 3
Rate of Change in Surface PH (decade^{-1}) Computed at Four Stations From WQMP Data, Continuous Monitoring Data, and Model Simulations (See Figure 1 for Station Locations; Stations are Numbered From North to South)

Station	Source	Jan	Feb	Mar	Apr	May	July	Aug	Sep	Oct	Nov	Dec
1	WQMP	N/A	N/A	**0.22± 0.10**	0.16± 0.08	0.09± 0.11	**–0.15± 0.07**	–0.06± 0.07	–0.16± 0.08	–0.03± 0.06	N/A	N/A
	CON MON	N/A	N/A	N/A	0.10± 0.05	0.11± 0.06	**–0.14± 0.03**	–0.04± 0.04	**–0.12± 0.03**	**–0.10± 0.02**	N/A	N/A
	All – Ref_{1985}	–0.00± 0.00	–0.00± 0.00	0.00± 0.00	0.01± 0.00	0.01± 0.00	–0.08± 0.00	–0.06± 0.00	–0.03± 0.00	–0.00± 0.00	0.01± 0.00	0.00± 0.00
2	WQMP	0.12± 0.09	0.01± 0.08	0.09± 0.05	0.13± 0.08	–0.04± 0.10	0.01± 0.04	–0.06± 0.05	–0.09± 0.05	0.01± 0.04	–0.01± 0.05	0.02± 0.07
	CON MON	–0.09± 0.10	**–0.40± 0.08**	**–0.50± 0.07**	**0.31± 0.09**	**–0.48± 0.12**	0.01± 0.05	**0.36± 0.04**	**0.29± 0.06**	**–0.13± 0.04**	**–0.36± 0.03**	**–0.32± 0.06**
	All – Ref_{1985}	–0.00± 0.00	–0.01± 0.00	–0.01± 0.00	0.00± 0.00	–0.04± 0.00	–0.08± 0.00	–0.05± 0.00	–0.04± 0.00	–0.02± 0.00	–0.00± 0.00	–0.01± 0.00
3	WQMP	–0.05± 0.08	0.02± 0.08	0.12± 0.07	0.16± 0.12	0.09± 0.10	–0.04± 0.05	–0.05± 0.06	–0.04± 0.05	0.01± 0.05	–0.05± 0.04	–0.07± 0.07
	CON MON	N/A	N/A	N/A	**–0.18± 0.05**	**–0.13± 0.05**	**0.19± 0.03**	–0.03± 0.03	**–0.05± 0.02**	**–0.06± 0.02**	N/A	N/A
	All – Ref_{1985}	–0.02± 0.00	–0.02± 0.00	–0.02± 0.00	–0.02± 0.00	–0.02± 0.00	–0.08± 0.00	–0.07± 0.00	–0.06± 0.00	–0.05± 0.00	–0.03± 0.00	–0.03± 0.00
4	WQMP	0.07± 0.14	0.04± 0.07	–0.06± 0.07	–0.15± 0.09	–0.03± 0.06	–0.02± 0.03	0.00± 0.02	0.03± 0.06	0.02± 0.05	–0.02± 0.04	0.11± 0.06
	CON MON	**–0.20± 0.02**	**–0.08± 0.03**	–0.03± 0.02	**–0.11± 0.02**	**–0.08± 0.01**	**–0.03± 0.01**	0.03± 0.01	0.03± 0.02	0.01± 0.02	**–0.04± 0.01**	–0.02± 0.02
	All – Ref_{1985}	–0.03± 0.00	–0.04± 0.00	–0.04± 0.00	–0.05± 0.00	–0.05± 0.00	–0.04± 0.00	–0.03± 0.00	–0.03± 0.00	–0.02± 0.00	–0.02± 0.00	–0.03± 0.00

In order to ensure that the longest and most consistent time series of pH data are used for trend calculation, WQMP pH data are from 1996 to 2018 and CONMON data are from mid-2000s to present. WQMP pH data (NBS scale) are generally measured once each month from October to March, and twice each month from April to September. CONMON data (NBS scale) are measured at a 15-minute interval, and daily mean values are used for trend calculations. In order to calculate the rate of change in modeled pH, surface pH from the Ref_{1985} simulation (1985–1989) is subtracted from the All sensitivity simulation (2015–2019); the resulting changes are then divided by three to obtain per decade trends. Bold numbers denote that the linear trend is significant ($p < 0.05$). Error bars for WQMP and CONMON rows are standard errors of the slope of the linear regression, and error bars for the model results (All – Ref_{1985}) represent the standard error of the daily estimates of the modeled trend in each month. If the standard error is greater than the value presented, the box is colored in grey even if the absolute value is greater than 0.05 decade^{-1}.

ΔpH (decade^{-1})	Color
Δ > 0.2	
0.2 ≥ Δ ≥ 0.05	
0.05 > Δ > –0.05	
–0.05 ≥ Δ ≥ –0.2	
Δ < –0.2	

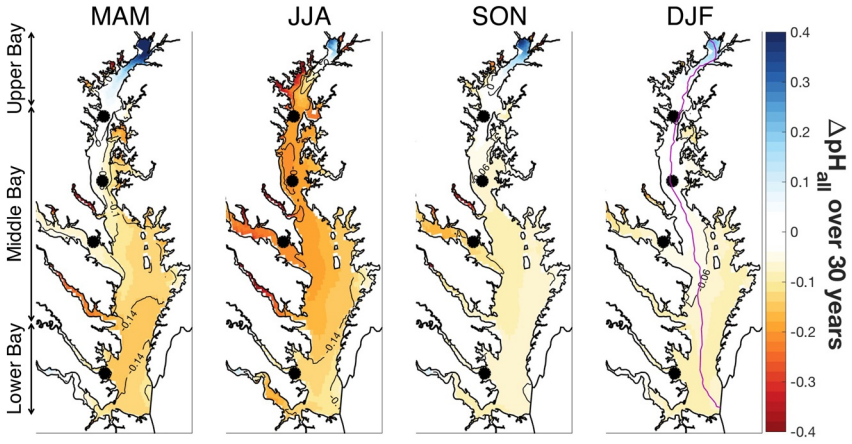

Figure 5. Overall changes in modeled surface pH due to all global and local drivers combined (ΔpH_{all} = All–Ref_{1985}). The purple line in the last panel represents the mainstem transect used in Figures 6–9. (MAM = spring, JJA = summer, SON = fall, and DJF = winter). Black circles show the locations of the model results at four stations in Table 3.

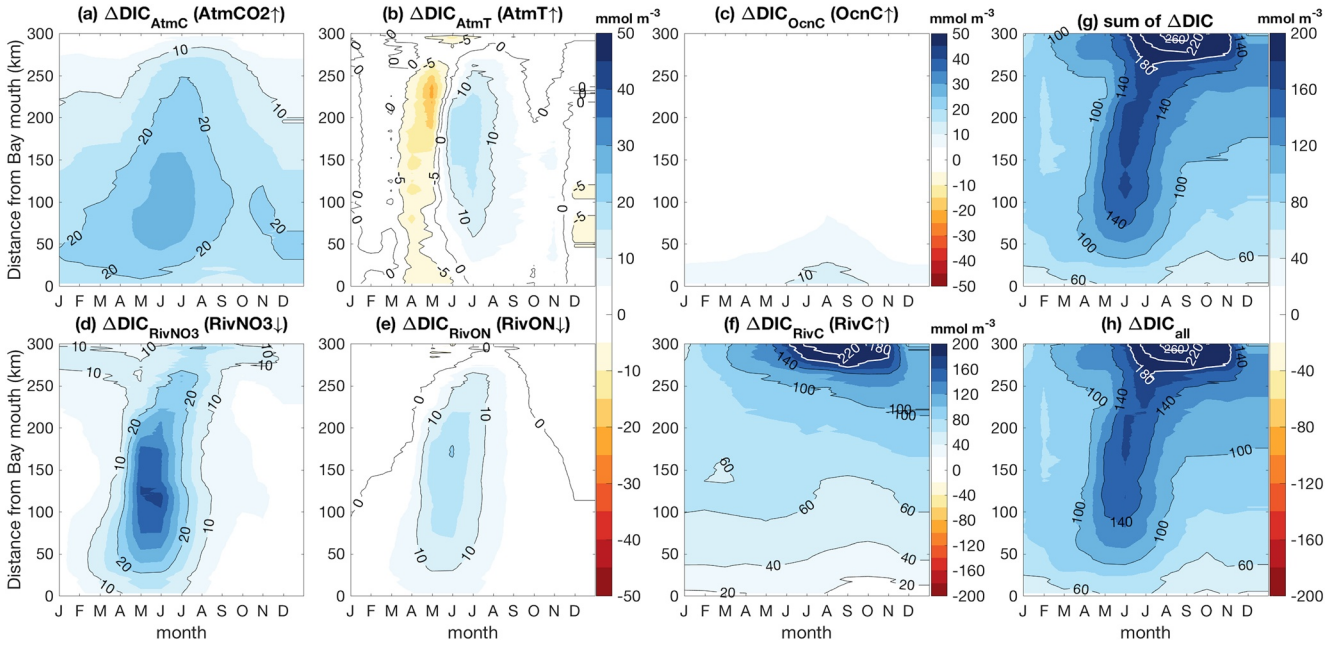

Figure 6. Seasonal cycle of the 30-year changes (Δ) in surface dissolved inorganic carbon (DIC (mmol m^{-3}) along the main stem due to: (a) increased atmospheric CO_2, (b) increased atmospheric thermal forcing, (c) increased oceanic DIC concentrations, (d) decreased riverine NO_3^- concentrations, (e) decreased riverine organic nitrogen concentrations, (f) increased riverine TA and DIC concentrations, (g) sum of the Δ in (a)–(f), and (h) all six drivers combined. Δ = sensitivity test–Ref_{1985}. Note change in color bar range in (f), (g) and (h).

the observed spatial variability relatively well, especially in the fall and winter. Overestimation of Ω_{AR} is most evident in the summer, again consistent with a modest overestimation of primary production, which results in greater seasonal variability in modeled Ω_{AR} compared to observations.

3.2. Quantifying Decadal Changes in Surface pH

Daily averaged CONMON pH data sometimes exhibit different trends than the monthly/semi-monthly WQMP data collected at adjacent locations (Table 3). At Station 1 where surface pH has been increasing in the spring and decreasing in the summer and fall in both datasets, the maximum reduction rate reaches ∼ −0.15 pH units $decade^{-1}$ in the summer and early fall. At Station 4, CONMON trends and WQMP trends agree relatively well, with significant reductions of −0.1 to −0.2 pH units $decade^{-1}$ especially in the spring and summer. At Stations 2 and 3, however, monthly trends calculated from the neighboring CONMON and WQMP data disagree with each other in most seasons. For example, these trends are opposite in sign during 8 of the 12 months at Station 2. This could partially be due to a sampling frequency issue. pH trends calculated from CONMON data that are resampled at the same time when WQMP data exist are quite different from the trends computed from daily averaged CONMON data (not shown). In addition, a simple linear regression model showed relatively low agreement between these two data sets ($R^2 < 0.55$; Figure S4); this is not unexpected considering that the uncertainty in each of these types of data can be up to 0.2 pH units, and indicates relatively low confidence in directly using CONMON and WQMP data to quantify how decadal trends in the Chesapeake Bay carbonate system vary month by month. However, given that WQMP pH data agree relatively well with high-quality pH data (Friedman et al., 2020) ($R^2 = 0.8$, not shown), historical WQMP pH data may be used to estimate interannual and spatial variability in the Chesapeake Bay carbonate system as long as they are paired with high-quality pH data and errors are estimated carefully (Herrmann et al., 2020).

The seasonal variability in surface pH trends is estimated from the model as well. In order to calculate the rate of change in modeled pH per decade over the past 30 years without biasing the results with interannual variability in atmospheric temperature and precipitation, surface pH from the Ref_{1985} simulation is subtracted from the All sensitivity simulation (Section 2.4; Table 1). The resulting decadal trend (ΔpH_{all}, Figure 5) is

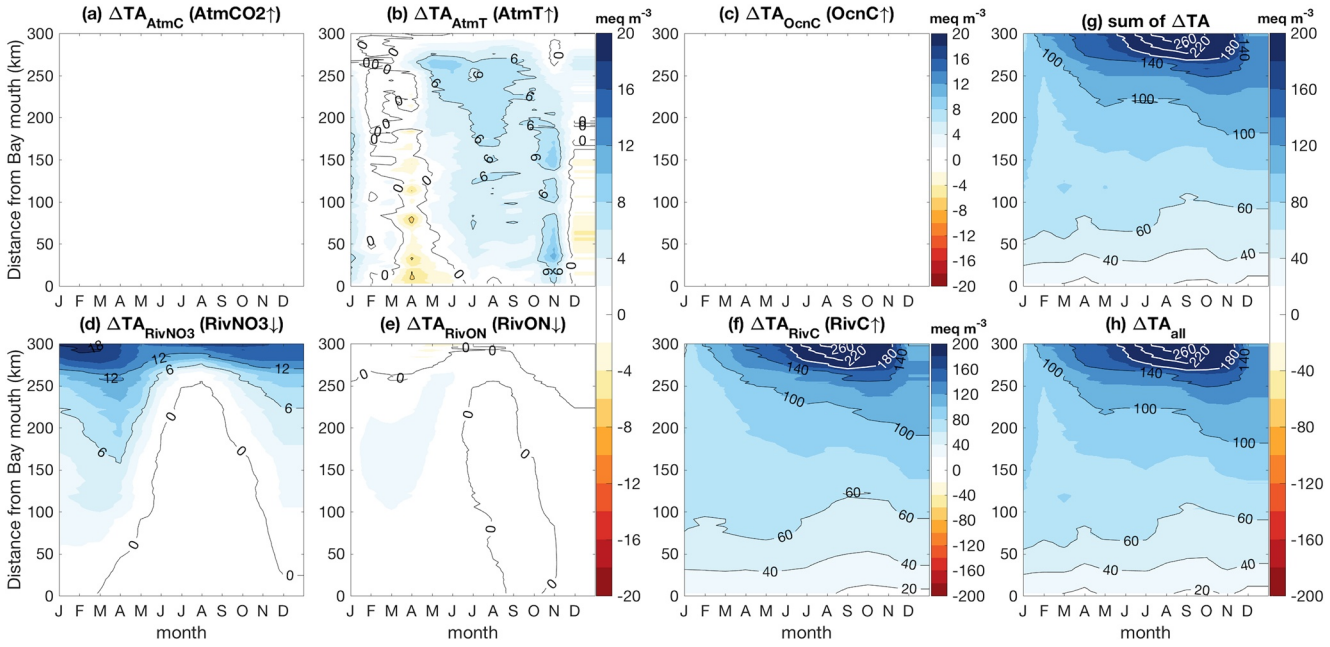

Figure 7. As in Figure 6, except for surface total alkalinity (meq m^{-3}). Note change in color bar range in (f), (g), and (h).

up to +0.13 pH units $decade^{-1}$ (+0.39 per 30 years) near the mouth of the Susquehanna River and decreases gradually toward the southern Bay to −0.02 to −0.08 pH units $decade^{-1}$ (−0.06 to −0.25 per 30 years). These 30-year changes in surface pH are usually smaller than the spatial variability in pH in the upper Bay, but they are comparable in the middle and lower Bay (Figure 4c). Moreover, this trend shows a strong seasonal cycle with the greatest reductions from April to October in the middle Bay and almost no trend in the winter, particularly north of the Potomac River (Figure 5). Overall, these changes in surface pH are not only apparent along the mainstem, but also expand into the Bay's shallow shoals and tributaries where calcifying

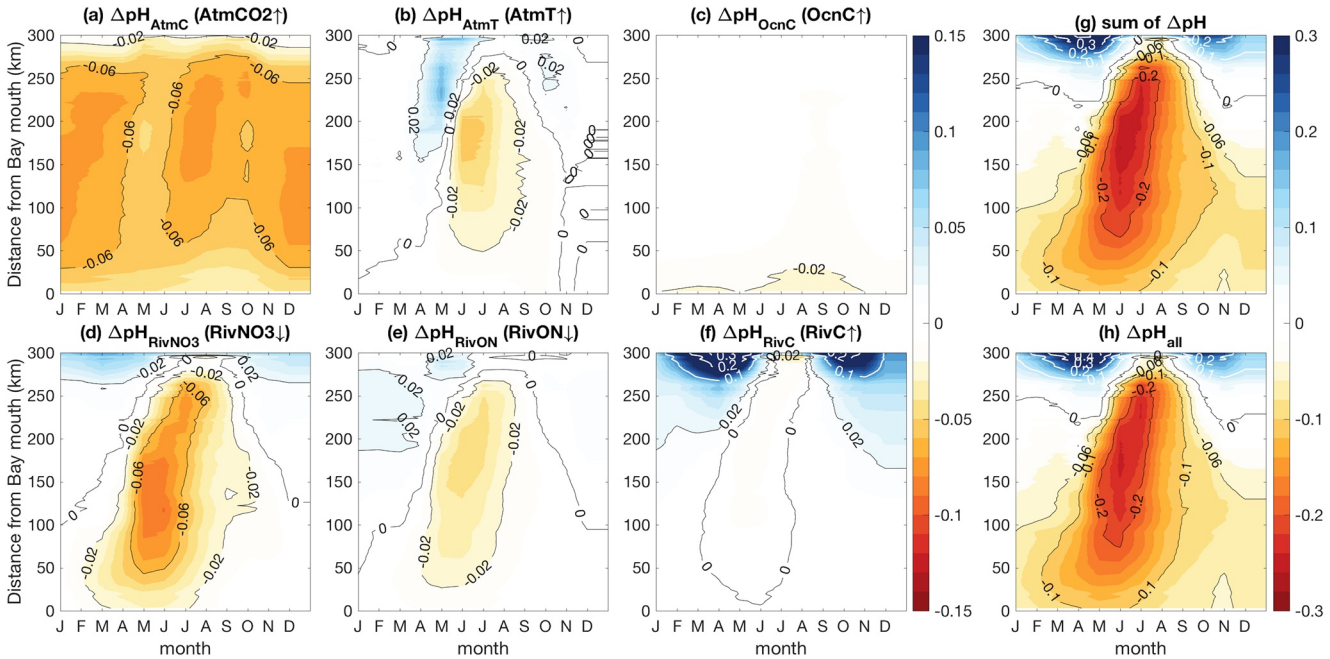

Figure 8. As in Figure 6, except for surface pH (total scale). Note change in color bar range in (g) and (h).

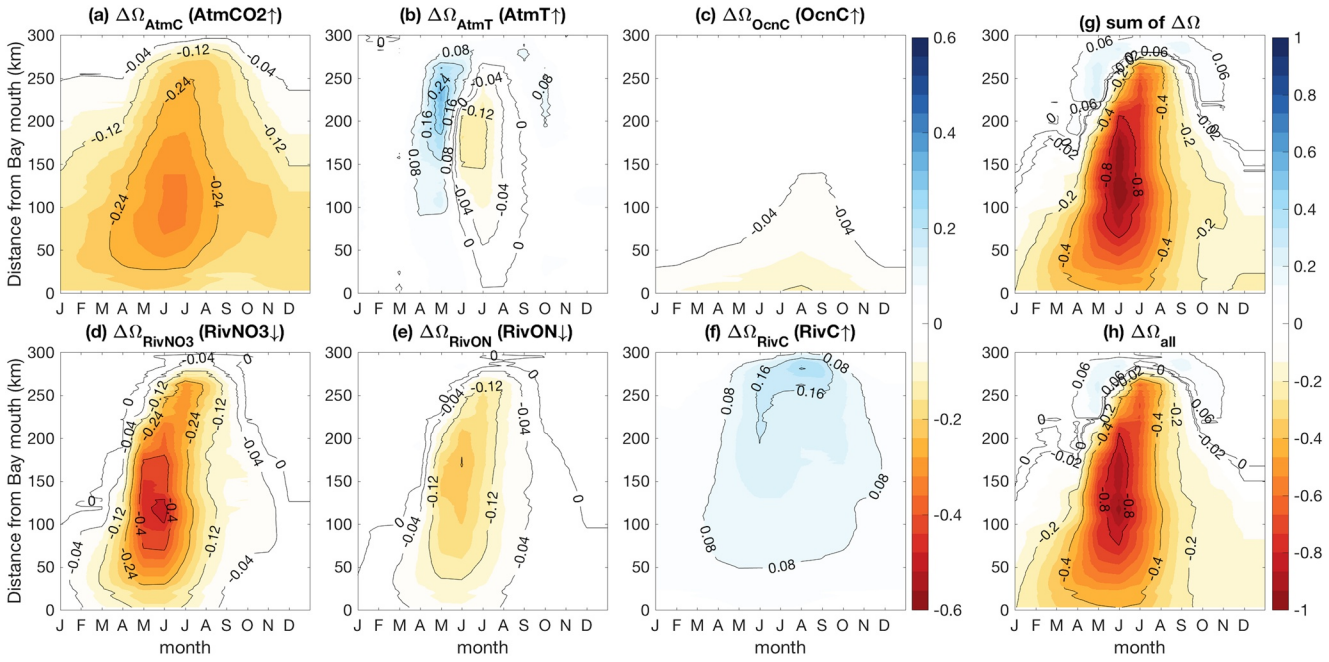

Figure 9. As in Figure 6 except for surface Ω_{AR}. Note change in color bar range in (g) and (h).

organisms typically reside. Additionally, modeled pH trends are consistent between the surface and bottom (Figure S5) especially in these shallow areas.

Given the discrepancy between the surface pH trends computed from the CONMON and WQMP datasets, the modeled pH trends are generally in reasonable agreement with the observed trends (Table 3). At Stations 1 and 2 (Table 3), the modeled rate of change in surface pH in the summer reaches −0.08 pH units decade^{-1} (−0.24 per 30 years, Figure 5), which is smaller than the maximum decrease calculated from the long-term data. In general, these modeled trends match the sign of the rate of change computed from either the CONMON and/or WQMP data, except that the model results do not show the increasing trend evident in the spring WQMP data at Station 1, though increasing trends are apparent farther north near the mouth of the Susquehanna River (Figure 5; Table S2). At Station 3, modeled pH trends agree with both datasets relatively well from August to January. At Station 4, the seasonal cycle of the decadal rate of change in modeled pH agrees with the seasonal variability showed in both the WQMP and CONMON data quite well. The rate of change in pH ranges from −0.03 to −0.05 pH units decade^{-1} (−0.09 to −0.15 per 30 years) in the spring and summer, and the values are smaller in the fall and winter. Additionally, surface pH trends are calculated from WQMP data and model simulations at 17 stations along the main channel of the Bay (Table S2). Both WQMP data and model results show overall increasing pH trends throughout the year at the northernmost stations near the mouth of the Susquehanna River. Toward the southern stations, however, both data and model show more negative trends, particularly in the summer months.

3.3. Mechanisms Causing Decadal Changes in the Carbonate System

This section summarizes the model-derived changes in the Chesapeake Bay carbonate system due to each individual driver and all six drivers combined (Section 2.4; Table 1). Unless otherwise noted, values reported in this section represent changes (Δ) over 30 years along the transect in the main channel of the Chesapeake Bay (purple line in Figure 5). These changes are plotted as mean annual time series to highlight their seasonal and spatial variability. The four variables include surface DIC (Section 3.3.1; Figure 6), surface TA (Section 3.3.2; Figure 7), surface pH (Section 3.3.3; Figure 8) and surface Ω_{AR} (Section 3.3.4; Figure 9). The relative impact of each driver is individually quantified by calculating the difference between the Ref_{1985} simulation and each sensitivity test (Section 2.4; Table 1). Subscripts of these changes (panels a–f in Figures 6–9) represent: increased atmospheric CO_2 concentrations (Δ_{AtmC}), increased atmospheric

thermal forcing (Δ_{AtmT}), increased oceanic DIC concentrations (Δ_{OcnC}), reduced riverine NO_3^- concentrations (Δ_{RivNO3}), reduced riverine organic nitrogen concentrations (Δ_{RivON}), and increased riverine DIC and TA concentrations (Δ_{RivC}). Furthermore, these individual changes are linearly added to obtain the sum of the changes (Figures 6g, 7g, 8g, and 9g), which are compared to the 30-year changes due to all drivers combined. Similar to the definition of the modeled changes in pH over the past 30 years (ΔpH_{all}, Section 3.2; Figure 8h), the 30-year changes in surface DIC, TA and Ω_{AR} due to all six drivers combined are defined as ΔDIC_{all} (Figure 6h), ΔTA_{all} (Figure 7h) and $\Delta\Omega_{all}$ (Figure 9h), which are calculated as the difference between the Ref_{1985} simulation and the All sensitivity simulation (Section 2.4; Table 1).

3.3.1. Seasonal Cycle of the 30-Year Change in Surface DIC

Each sensitivity experiment shows a distinct pattern in the changes in surface DIC over the past three decades. For example, ΔDIC_{AtmC} ranges between +10 and + 25 mmol m^{-3}, with slightly greater values in the summer and middle Bay (Figure 6a). Over the same time period, ΔDIC_{AtmT} is positive in the summer (up to +15 mmol m^{-3}), and negative (−5 to −10 mmol m^{-3}) in the spring (Figure 6b). Largest ΔDIC_{OcnC} occurs in the lower Bay during the summer (∼10 mmol m^{-3}), with smaller values in closer proximity to the inner Chesapeake Bay (e.g., there are almost no changes in the middle and upper Bay; Figure 6c). ΔDIC_{RivNO3} reaches +30 mmol m^{-3} in the summer in the middle Bay, but it is barely noticeable in cooler seasons (Figure 6d). Similarly, ΔDIC_{RivON} is only apparent in the summer, with values of up to +15 mmol m^{-3} in the middle Bay (Figure 6e). Maximum ΔDIC_{RivC} is found in waters adjacent to the Susquehanna River in late summer (+240 mmol m^{-3}); these changes are smaller and seasonally uniform (+30 mmol m^{-3}) near the mouth of the Bay (Figure 6f).

There are strong seasonal and spatial variations in the 30-year changes in Chesapeake Bay surface DIC (i.e., ΔDIC_{all}, Figure 6h). Over the past three decades, ΔDIC_{all} is positive throughout the Bay, increasing by up to +260 mmol m^{-3} in the upper Bay and by a lesser amount nearer to the Bay mouth (+60 mmol m^{-3}). In the middle Bay, ΔDIC_{all} is greatest in the late spring and summer, with a relatively large annual range of ∼80 mmol m^{-3}. The seasonal variability of ΔDIC_{all} is even greater (∼180 mmol m^{-3}) in the upper Bay, with values peaking in the late summer and early fall. The magnitude of these changes is dominated by the increase in riverine DIC and TA, while results from other experiments primarily contribute to the seasonal variability of ΔDIC_{all} in the middle and lower Bay. For example, about half of the seasonal variability in ΔDIC_{all} is caused by ΔDIC_{RivNO3} in the middle Bay. Additionally, the sum of the changes due to each individual driver (Figure 6g) reproduces the spatiotemporal pattern of ΔDIC_{all} (Figure 6h) quite well.

3.3.2. Seasonal Cycle of the 30-Year Change in Surface TA

Changes in surface TA due to increased riverine TA and DIC concentrations (ΔTA_{RivC}) display the largest values, while other experiments show much smaller changes over the past three decades. Specifically, ΔTA_{AtmC} and ΔTA_{OcnC} are zero throughout the Chesapeake Bay (Figures 7a and 7c). The value of ΔTA_{AtmT} is positive (<10 meq m^{-3}) in the summer and fall, while being negative (up to −4 meq m^{-3}) in the winter and spring (Figure 7b). ΔTA_{RivNO3} shows the second largest changes throughout the Bay among all six sensitivity experiments, with the largest values occurring in the upper Bay (+18 meq m^{-3}) and little changes in the middle and lower Bay especially in the summer (Figure 7d). Additionally, ΔTA_{RivON} is less than 2 meq m^{-3} throughout the Bay (Figure 7e). As was the case for DIC, the value of ΔTA_{RivC} peaks around +260 meq m^{-3} and exhibits a notable seasonal cycle in the upper Bay; its value decreases gradually to +40 meq m^{-3} in the lower Bay (Figure 7f).

Over the past 30 years, changes in Chesapeake Bay surface TA (i.e., ΔTA_{all}, Figure 7h) resemble the magnitude as well as the spatial and temporal patterns of ΔTA_{RivC} (Figure 7f). Similar to ΔDIC_{all}, the greatest value of ΔTA_{all} is also in the upper Bay (+280 meq m^{-3}) and its value decreases to +40 meq m^{-3} in the lower Bay (Figure 7h). However, ΔTA_{all} has much smaller seasonal variability than ΔDIC_{all} except in the upper Bay where its seasonal range is similar (∼200 meq m^{-3}). Furthermore, these changes in surface TA are almost linearly additive (Figure 7g), with ΔTA_{RivC} primarily contributing to these decadal changes and other experiments displaying much smaller or no changes.

3.3.3. Seasonal Cycle of the 30-Year Change in Surface pH

Each sensitivity experiment displays a distinct spatiotemporal influence on surface pH in the Chesapeake Bay. For example, ΔpH_{AtmC} is relatively consistent over the seasons, with values of −0.05 to −0.07 pH units throughout most of the main channel (Figure 8a). Additionally, ΔpH_{AtmT} switches sign seasonally, with values of +0.02 to +0.07 pH units in the spring in the upper Bay and values of up to −0.05 pH units in the summer in the middle Bay (Figure 8b). The value of ΔpH_{OcnC} is generally near −0.02 pH units in the lower Chesapeake Bay, and it diminishes substantially toward the middle and upper Bay (e.g., very small changes 50 km from the Bay mouth, Figure 8c). In the upper Bay, ΔpH_{RivNO3} is positive (up to +0.05 pH units) except in the summer. In the middle and lower Bay, ΔpH_{RivNO3} ranges from near zero in the winter to −0.08 pH units in the summer (Figure 8d). ΔpH_{RivON} has a similar spatiotemporal pattern as ΔpH_{AtmT}, here again the most negative values (−0.04 pH units) are found in the middle Bay during the summer (Figure 8e). Unlike other sensitivity experiments, ΔpH_{RivC} is almost always positive throughout the Chesapeake Bay, with maximum values found in the spring in the upper Bay (+0.3 pH units; Figure 8f; these maximum values are represented by the white contours in the panel).

There are evident spatiotemporal variations in the decadal changes in surface pH over the past 30 years (i.e., ΔpH_{all}, Figure 8h). Overall, ΔpH_{all} is negative throughout most of the Bay but positive in the northernmost reaches of the Bay where it ranges between +0.2 to +0.4 pH units in the fall, winter and spring but is near zero in the summer. The minimum ΔpH_{all} occurs in the middle Bay in the late spring and early summer with values reaching −0.24 pH units. Specifically, ΔpH_{AtmC} and ΔpH_{RivNO3} are the two largest components contributing to ΔpH_{all}, and ΔpH_{RivNO3} is responsible for nearly half of the temporal variability in ΔpH_{all} in the middle Bay.

3.3.4. Seasonal Cycle of the 30-Year Change in Surface Ω_{AR}

The seasonal cycle of the 30-year change in surface Ω_{AR} varies substantially among the six individual sensitivity experiments (Figures 9a–9f). For example, surface $\Delta\Omega_{AtmC}$ is negative throughout the year, with the greatest changes reaching −0.3 in the middle Bay in the summer (Figure 9a). Unlike $\Delta\Omega_{AtmC}$, $\Delta\Omega_{AtmT}$ is only apparent in the summer (reaches −0.1) and spring (up to +0.2) in the middle Bay (Figure 9b). Another minor 30-year change is $\Delta\Omega_{OcnC}$, which only reaches −0.05 to −0.1 near the mouth of the Bay (e.g., Figure 9c). In contrast, $\Delta\Omega_{RivNO3}$ reaches −0.5 in the late spring and early summer, but is only around −0.05 in the winter. Spatially, $\Delta\Omega_{RivNO3}$ is the smallest near the river and the Bay mouth (Figure 9d). $\Delta\Omega_{RivON}$ shares similar spatial and temporal patterns as $\Delta\Omega_{RivNO3}$, but to a lesser extent (e.g., with values reaching −0.2 in the summer; Figure 9e). Counteracting these changes, $\Delta\Omega_{RivC}$ ranges from +0.08 to +0.2 throughout much of the main channel (Figure 9f).

The mean annual time series of the decadal changes in surface Ω_{AR} (i.e., $\Delta\Omega_{all}$, Figure 9h) shows substantial seasonal and spatial variability. The pattern of $\Delta\Omega_{all}$ is similar to that of ΔpH_{all}, but varies between −0.9 and + 0.1, with small positive values found only in the upper Bay and the most negative values found in the summer throughout the middle and lower Bay (Figure 9h). Regardless of the nonlinearity in the carbonate system, $\Delta\Omega_{all}$ agrees well with the sum of the changes calculated from each individual sensitivity experiment (Figure 9g). Specifically, $\Delta\Omega_{AtmC}$ and $\Delta\Omega_{RivNO3}$ accounts for most of the variability in $\Delta\Omega_{all}$, while $\Delta\Omega_{RivC}$ plays a minor counteracting role.

4. Discussion

The Chesapeake Bay surface carbonate system has seen substantial change over the past three decades. Our model experiments suggest that multiple drivers have directly modified physical and/or biogeochemical processes, producing distinct impacts on TA, DIC, pH and Ω_{AR}. Specifically, global-scale drivers include increased atmospheric CO_2 concentrations, increased atmospheric thermal forcing and increased oceanic DIC concentrations; local-scale drivers include reduced riverine NO_3^- and organic nitrogen concentrations, and increased riverine DIC and TA concentrations. Causes of the impacts on the Chesapeake Bay carbonate system due to each individual driver over the past three decades are discussed in Section 4.1 (global drivers) and Section 4.2 (local drivers). These changes are compared to previous studies in Section 4.3, which includes decadal trends in other coastal regions and uncertainties associated with the glass electrode pH data.

4.1. Relative Impacts of Global-Scale Drivers on the Chesapeake Bay Carbonate System Over the Past 30 Years

Elevated atmospheric CO_2 concentration over the past three decades has been the primary global-scale driver impacting the Chesapeake Bay carbonate system via modification of the air-water CO_2 flux. Atmospheric CO_2 records at Mauna Loa (Keeling & Keeling, 2017) show seasonally consistent increasing trends over the past three decades, with only a slightly lower change in the spring and summer (+56.5 ppm) compared with that in the winter (+57.5 ppm). This motivated the use in this study of a seasonally independent change (+57 ppm). In general, the upper Chesapeake Bay outgasses CO_2 throughout the year, while the middle Bay takes up CO_2, which likely reflects a shift from net heterotrophy in the upper Bay to net autotrophy in the middle Bay (Chen et al., 2020; Friedman et al., 2020; Herrmann et al., 2020; Kemp et al., 1997). Increased CO_2 concentrations in the atmosphere result in less outgassing in the upper Bay and more uptake in the middle Bay (St-Laurent et al., 2020). This change in air-water CO_2 exchange increases surface DIC (+5 to +25 mmol m^{-3} per 30 years, Figure 6a) but not TA (Figure 7a), and decreases surface pH (−0.02 to −0.07 pH units per 30 years, Figure 8a) and Ω_{AR} (−0.05 to −0.32 per 30 years, Figure 9a). Moreover, the increase in surface DIC and the decrease in surface Ω_{AR} have a clear spatiotemporal pattern, with greatest changes occurring when and where productivity is high (in the summer and in the mid-Bay).

Variability in biological modifications and seawater chemistry, rather than changing atmospheric CO_2, explains the spatiotemporal patterns of decadal changes in the Chesapeake Bay surface carbonate system. In the summer and in the middle Bay, surface DIC and pCO_2 levels are lower than other seasons and regions due to high primary production (Brodeur et al., 2019; Friedman et al., 2020; Herrmann et al., 2020). For a seasonally uniform increase in atmospheric CO_2, there can be more uptake of CO_2 in the summer and in the middle Bay where there is a biologically driven undersaturation of pCO_2 relative to the atmosphere, which leads to greater increases in surface DIC (Figure 6a). Another way to resolve these changes in surface DIC is by using the modeled Revelle factor, DIC concentrations, pCO_2 concentrations, and the changes in pCO_2 at the surface. For example, in the upper Bay where DIC concentrations are low while pCO_2 levels and the Revelle factor are high, the increases in surface DIC are smaller (Figure 6a). As a result, decadal increases in surface DIC due to increased atmospheric CO_2 are higher in the summer and in the middle Bay, while those changes are lowest in the upper Bay (Figure 6a). Because of the high sensitivity of Ω_{AR} to the TA-to-DIC ratio (Cai, Feely, et al., 2020; Takahashi et al., 2014), the reduction in Ω_{AR} (Figure 9a) follows the spatiotemporal patterns of the increases in DIC (Figure 6a) and the decreases in CO_3^{2-}. The reduction in surface pH due to increased atmospheric CO_2 has relatively small seasonality in most of the Bay's main channel (Figure 8a), ranging from −0.06 to −0.07 pH units per 30 years, which is comparable with the rate of pH reduction observed in the open ocean (e.g., Takahashi et al., 2014). Since the sensitivity factor of pH to the changes in DIC is higher when salinity is lower (Cai, Feely, et al., 2020), and the increase in DIC due to elevated atmospheric CO_2 shows smaller values in the upper Bay where salinity is lower (Figure 6a), the resulting changes in surface pH has relatively small spatial variability. Parameters related to the air-water CO_2 flux, such as CO_2 solubility and gas transfer velocity, vary substantially throughout the year given the strong seasonal variability in temperature (>25 °C) in the Chesapeake Bay (Figure S6). However, these two parameters have opposite responses to water temperature (Figure S6) and thus the seasonal variations in decadal changes in surface DIC is likely unrelated to the temperature impacts on the air-water CO_2 flux.

Increased atmospheric thermal forcing has less of an impact on the Chesapeake Bay carbonate system than that from increased atmospheric CO_2, and the spatiotemporal patterns of the resulting decadal changes are quite different. As described in Section 2.4, changes in the atmospheric thermal forcing vary substantially throughout the year, yet the Chesapeake Bay continues to warm in all months of the year (Ding & Elmore, 2015; Hinson et al., 2021; Muhling et al., 2018). Increased water temperature promotes earlier phytoplankton growth and increases primary production in the spring especially in the upper Bay (Figure S7b), which results in less DIC (Figure 6b) and slightly more oxygen at the surface in April (Figure S8b). Additionally, these changes are reflected in surface pH and Ω_{AR}; both variables are higher in the upper Bay in the spring (Figures 8b and 9b) due to the reduction in surface DIC. In the summer, however, there are no apparent trends in primary production due to increased atmospheric thermal forcing. Increased water temperature enhances respiration and production while decreasing gas solubility, resulting in counteracting impacts on DIC. Because respiration increases more than production when temperatures rise (Lomas

et al., 2002), the increase in DIC in the summer (Figure 6b) is likely a net effect of enhanced respiration and production opposed by decreased CO_2 solubility, which results in net reductions in summer pH and Ω_{AR} (with values reaching −0.05 pH units and −0.12 per 30 years, respectively; Figures 8b and 9b). Additionally, increased temperature decreases pH and increases Ω_{AR} by modifying the dissociation constants and calcium carbonate solubility, e.g., about −0.01 pH units and <+0.01 of change in pH and Ω, respectively, given a +0.7 °C increase in surface water temperature over the past 30 years (Hinson et al., 2021). However, these impacts are much smaller than those due to biological processes.

The final global-scale driver is the increased oceanic DIC concentrations in the MAB, primarily caused by the increase in atmospheric CO_2 (Xu et al., 2020). Near the Bay mouth, this has slightly increased DIC (Figure 6c) and correspondingly decreased pH and Ω_{AR} (Figures 8c and 9c) over the past 30 years. As expected, the impact from the Atlantic Ocean on the Bay lessens with distance from the Bay mouth. Because of the long distance between the Bay mouth and the model open boundary located in the MAB where oceanic DIC concentrations are increased, the rate of DIC increase near the Bay mouth (up to +10 mmol C m^{-3} per 30 years in the summer) is roughly one third of the rate calculated in the MAB (Xu et al., 2020). However, the 30-year increase in surface DIC due to all drivers combined reaches +60 mmol C m^{-3} in the same region of the Bay (Figure 6h).

4.2. Relative Impacts of Local-Scale Drivers on Chesapeake Bay Carbonate System Over the Past 30 Years

Among the local-scale drivers analyzed here, NO_3^- reductions from the Chesapeake Bay watershed are responsible for the largest trends in pH and Ω_{AR} over the past 30 years. Reduced riverine NO_3^- concentrations impact the carbonate system by (1) directly increasing surface TA and by (2) decreasing primary production and hence decreasing surface TA. Since NO_3^- is the conjugate base of a strong acid (HNO_3), decreased NO_3^- concentrations directly increase TA and correspondingly result in higher pH and Ω_{AR}, especially in the upper Bay. In contrast, biological responses of the carbonate system to NO_3^- reductions have the opposite sign and are associated with substantial seasonal variability. Since nitrogen limits primary production throughout much of the Chesapeake Bay (except where light is the limiting factor in the upper Bay; Kemp et al., 2005), NO_3^- reductions (Moyer & Blomquist, 2020; Zhang et al., 2015) decrease primary production and thus leave more DIC and less TA in surface waters, subsequently decreasing both surface pH and Ω_{AR}. From the late spring to early fall, nitrogen is most limiting (Kemp et al., 2005) and primary production rates are usually highest (Harding et al., 2002; Son et al., 2014); therefore, biological responses to NO_3^- reductions are greatest during this time. Together, biological impacts outweigh the direct impacts from NO_3^- reductions especially in the middle and lower Bay, resulting in net increases in DIC and net decreases in TA, pH and Ω_{AR} at the surface (Figures 6, 7, 8, and 9d). However, in the upper Bay where light limits production and nitrogen is replete, the direct impact of reduced riverine NO_3^- dominates and results in slight increases in TA and pH. Furthermore, these changes associated with reduced riverine NO_3^- inputs account for nearly half of the changes in surface DIC, pH and Ω_{AR} due to all six drivers combined, especially in the middle Bay (Figures 6h, 8h and 9h).

Riverine organic nitrogen inputs, including both labile and refractory components, have also been reduced over the past 30 years and also impact the Chesapeake Bay carbonate system most during the summer. Decreased organic nitrogen initially yields less decomposition (and higher oxygen concentrations, Figure S8e) in the upper Bay, which then lowers NH_4^+ levels (Fig. S9e) and primary production (Figure S7e), ultimately contributing to an increase in surface DIC and reductions in surface pH and Ω_{AR}. Reductions in riverine organic nitrogen have spatiotemporal impacts on the carbonate system that are similar to but lower in magnitude than those resulting from reductions in NO_3^- for two reasons: (1) the 30-year reductions in organic nitrogen are smaller than those of NO_3^- (Figure 2b) and (2) the refractory component of organic nitrogen does not impact the biogeochemical processes. Specifically, the increase in surface DIC due to reductions in organic nitrogen (Figure 6e) is about half the value of the NO_3^- counterpart; TA barely changes and the reductions in pH and Ω_{AR} are two times smaller (Figures 8e and 9e). As was the case for increased atmospheric thermal forcing, these decadal changes due to decreased riverine organic nitrogen inputs only add a slight seasonal variability to the overall changes in the Chesapeake Bay surface carbonate system (Figures 6h, 7h, 8h, and 9h).

Increased riverine TA and DIC input is the local-scale driver that has the greatest impact on Chesapeake Bay surface TA and DIC concentrations over the past 30 years. The analysis of long-term USGS data finds annual increasing trends in riverine TA and DIC concentrations that are similar to previous studies (Najjar et al., 2020; Raymond & Oh, 2009), and underscores clear seasonal patterns in both TA and DIC trends over the past three decades in the two largest tributaries of the Bay (i.e., the Susquehanna and the Potomac River). Relatively large increasing trends are found from July to December in the Susquehanna River, and from December to February in the Potomac River (Figure 2c). Given that the Susquehanna River accounts for more than 50% of the freshwater discharge entering the Bay, and the Potomac River fall line is far from the mainstem, decadal changes in surface TA and DIC are dominated by changes in the Susquehanna River. These decadal increases are greatest in the upper Bay with large seasonality (80–260 meq m^{-3} and 80–240 mmol m^{-3} per 30 years for surface TA and DIC, respectively; Figures 6f and 7f), and decrease rapidly toward the middle and lower Bay. TA observations in the upper and middle Bay also show increases over the same time period (Herrmann et al., 2020) and in prior decades (Najjar et al., 2020). It is noteworthy that increases in riverine TA and DIC drive the increases in Chesapeake Bay surface TA and DIC over the past three decades (Figures 6h and 7h), yet the large seasonality in the increase in DIC in the mid- and lower Bay is a combination of the various drivers discussed above.

The 30-year increase in riverine TA and DIC also increases surface pH and Ω_{AR}, especially in the upper Bay. TA concentrations in the Susquehanna River have been increasing at faster rates than DIC year-round, with the ratio between their decadal increases ranging from ~1.2 in the summer to over 1.6 in the spring and winter. Therefore, in the upper Bay, the resulting increase in surface pH is lowest in the summer (<0.1 pH units per 30 years), and ranges from +0.1 to +0.3 pH units per 30 years in the spring. Because of the increase in surface CO_3^{2-} concentration, surface Ω_{AR} has increased throughout the Bay with maximum values of 0.2 per 30 years in the upper Bay. However, other drivers such as increased atmospheric CO_2 counteract the increases in pH and Ω_{AR} in this region, resulting in a near zero change in pH (Figure 8h) and a small increase in Ω_{AR} (Figure 9h; 0–0.06 per 30 years) in the summer when all drivers are considered together.

4.3. Comparison With Previous Studies of Decadal Carbonate System Changes in Coastal Regions

Due to their proximity to land and their resulting sensitivity to changes in terrestrially derived inputs, the estuarine carbonate system is likely to change at much different rates than the open ocean carbonate system. Takahashi et al. (2014) summarized the mean rate of change in the carbonate system at time-series stations (1980s–2010s) in the Pacific, Atlantic and subantarctic Southern Oceans and suggested that the mean acidification rate in the global ocean primarily results from the atmospheric CO_2 increase, with other physical and biological processes having smaller impacts over this period. In contrast, in coastal environments local changes in water temperature, salinity and nutrients have been shown to directly effect changes in the carbonate system by modifying the chemical equilibrium, physical processes and biogeochemical rates (Carstensen & Duarte, 2019; Cai, Feely, et al., 2020, Cai, Xiu, et al., 2020).

Because of the variety of anthropogenic drivers impacting coastal environments, the resulting long-term changes in the carbonate system of coastal waters vary substantially across ecosystems. For example, alongshore winds (Sydeman et al., 2014) and decadal climate variability (e.g., Pacific Decadal Oscillation) determine upwelling strength in the California Current Ecosystem, potentially leading to enhanced or mitigated signals of coastal acidification (Osborne et al., 2020). Salisbury and Jönsson (2018) analyzed long-term data and model products in the Gulf of Maine and similarly found that ocean circulation and rapid warming were substantially impacting coastal acidification via an event related to a retreat of the Labrador Current and a northward shift of the Gulf Stream (Saba et al., 2016). A combination of increased outgassing due to warming as well as increases in salinity and TA eventually caused slower pH reductions and increased Ω_{AR} between 2004 and 2014. In contrast, local changes in river discharge and riverine TA-to-DIC ratios have had opposite impacts on the buffering capacity of two North Carolina estuarine systems, resulting in distinct decadal pH trends in the two systems (Van Dam & Wang, 2019). As highlighted in this study, the Chesapeake Bay is experiencing changes in coastal acidification due not only to increasing atmospheric CO_2 concentrations directly, but also due to changes in terrestrial inputs (less nitrogen but more TA and DIC).

In contrast, increased DIC inputs through the Bay mouth have had little impact on surface pH and Ω_{AR} in the Bay.

Our results can also be compared with those of Shen et al. (2020) who examined spring and summer trends in Chesapeake Bay surface pH and Ω_{AR} using a similar biogeochemical-circulation model. They found increasing trends in the upper Bay and decreasing trends in the middle Bay. The pH trends identified here are similar in magnitude to those of Shen et al. (2020); however, our study found a faster decreasing rate of surface Ω_{AR} in the middle Bay due to greater impacts from biological processes (e.g., nutrient reduction). Additionally, both studies suggest a smaller spatial extent of increasing pH trends in the upper Bay than are shown by summer WQMP pH observations. This may be related to the recovery of submerged aquatic vegetation beds in the shallow shoals near the Susquehanna River, due to past and ongoing nutrient management efforts in this region (Lefcheck et al., 2018). Recovery of these aquatic plants can result in decadal increases in the precipitation of carbonate minerals and daytime pH in the upper Bay, especially in the summer when photosynthesis rates are high (Su et al., 2020). Including the impacts of submerged aquatic vegetation and calcium carbonate cycling in our future modeling efforts may likely help improve the estimation of the decadal carbonate system trends in the upper Bay.

It is more challenging to compare the results of this modeling study with existing observationally derived trends. For example, a change in measurement protocols around 1996 prohibits a comparison of pH data collected before and after this date (see Herrmann et al., 2020 for details). The analysis in the present study thus avoids using pH data from those early years, but there remains a possibility that the change in methodology after 1996 contributed to artificially high pH values in the lower Chesapeake Bay in the analyses of Waldbusser et al. (2011). Furthermore, the disagreement between the trends calculated from the two data sources (CONMON and WQMP) complicates assessment of trends directly calculated from these glass electrode pH data, which are inherently associated with large uncertainties. These historical pH data have been recently used to evaluate changes in air-sea CO_2 exchange after rigorous treatment of errors (Herrmann et al., 2020). This highlights the ongoing need to obtain consistent high-quality pH measurements to assess robust trends in the carbonate system (Goldsmith et al., 2019; Sutton & Newton, 2020). Additional observations on benthic processes that can influence the surface carbonate system via vertical mixing, such as sulfate reduction in anoxic bottom waters and sediments as well as the resulting oxidation of $HS^-$and NH_4^+ outfluxes (Cai et al., 2017), are also critical for improving model parameterizations. Including such processes in our modeling system will enhance model realism, and will ultimately lead to better estimates of long-term trends in the Chesapeake Bay carbonate system.

5. Summary and Conclusions

Over the past several decades, multiple anthropogenic drivers have caused a complex pattern of change in the carbonate system of coastal regions. The spatiotemporal variability of these changes is much greater than that observed in the open ocean, due to a combination of influences from the land, atmosphere and ocean. For example, this modeling study has demonstrated that in the freshest portion of the upper Chesapeake Bay, decadal change is primarily caused by seasonally varying increases in TA and DIC concentrations from the Susquehanna River, with other drivers only contributing to decadal changes that are one to two orders of magnitude smaller. In contrast, throughout the rest of the Bay, globally elevated atmospheric CO_2 concentrations and locally reduced riverine nutrient concentrations play critical and nearly equal roles in driving decadal trends in the surface carbonate system, while other drivers (e.g., increased atmospheric thermal forcing and oceanic DIC concentrations) play a less important role. Moreover, in this region the 30-year decreases in pH and Ω_{AR} show significant seasonal variability with the greatest changes generally aligning with the spring and summer shellfish production season.

Our results quantifying the relative importance of various drivers of coastal acidification provide critical information for management efforts aiming to control the risks of future acidification. Unlike changes in global drivers, such as increasing atmospheric temperature and CO_2 concentrations, nutrient loading can be locally managed through the implementation of TMDLs. In fact, the reduction of nutrient inputs to the Chesapeake Bay has not only led to some success in controlling hypoxia in the Chesapeake Bay (Irby & Friedrichs, 2019; Ni et al., 2020), but is likely improving pH and Ω_{AR} in the deep channel as well (Shen

et al., 2020). These improvements in bottom pH in the deep mainstem Bay are beyond the scope of this study, but should be investigated in more detail in the future. In contrast, the results of this study demonstrate that nutrient reductions may be reducing pH and Ω_{AR} at the surface, particularly during the most productive shellfish months (i.e., April to September). This may be pushing calcifying organisms to their physiological limits, with the resulting negative impacts strongly affecting early life history stages (Gobler & Talmage, 2013; Gobler et al., 2014; Talmage & Gobler, 2011; Waldbusser et al., 2013). Since the shellfish industry is critical to many local economies, such as that in the Chesapeake Bay watershed (Hudson, 2019), a reduction in shellfish production can have serious economic consequences.

In this study, decreases in surface pH and Ω_{AR} associated with nutrient reductions highlight that this estuarine ecosystem is returning to a more natural condition, e.g., a condition when anthropogenic nutrient input from the watershed was lower. However, increased atmospheric CO_2 is simultaneously accelerating the rate of change in pH and Ω_{AR}, exerting increased stress on estuarine calcifying organisms. The combined effects of these local- and global-scale drivers suggest that calcifying organisms in coastal surface waters are likely facing faster decreasing rates of pH and Ω_{AR} than those in open ocean ecosystems. As nutrient reduction efforts to improve coastal water quality continue and expand in the future, controlling the emissions of anthropogenic CO_2 globally becomes increasingly important for the shellfish industry and the ecosystem services it provides (Doney et al., 2020). In addition, continuing to expand high-quality carbonate system monitoring networks in these coastal systems is becoming ever more critical for accurately quantifying robust acidification trends, and for furthering our understanding of long-term change in coastal carbonate systems.

Data Availability Statement

Model outputs of this work are publicly available through W&M's Digital Archive at https://doi.org/10.25773/6087-bj68. This is Virginia Institute of Marine Science contribution 4011.

Acknowledgments
This work has been supported by the National Science Foundation (OCE-1537013, OCE-1536996), the Mid-Atlantic Sea Grant/NOAA OAP Graduate Research Fellowship (NA14OAR4170093, NA18OAR4170083) and the Virginia Institute of Marine Science Foundation. Additional funding comes from the National Oceanic and Atmospheric Administration's Ocean Acidification Program under award NA18OAR0170430 to the Virginia Institute of Marine Science. The authors thank Scott Doney, Emily Rivest and Karen Hudson for helpful comments on an initial version of this manuscript. We thank Jeremy Testa and Qian Zhang for their advice on early stages of the project. Many thanks to Edward Stets at the United States Geological Survey for providing riverine alkalinity and dissolved inorganic carbon data products. The authors thank the Chesapeake Bay Program Watershed Modeling team for providing model forcing files from the Chesapeake Bay Watershed Model. This work used High Performance Computing facilities at the William & Mary, which are supported by the National Science Foundation, the Commonwealth of Virginia Equipment Trust Fund and the Office of Naval Research.

References

Bever, A. J., Friedrichs, M. A. M., & St-Laurent, P. (2021). Real-time environmental forecasts of the Chesapeake Bay: Model setup, improvements, and online visualization. *Environmental Modelling & Software*, *140*, 105036. https://doi.org/10.1016/j.envsoft.2021.105036

Borges, A. V., & Gypens, N. (2010). Carbonate chemistry in the coastal zone responds more strongly to eutrophication than ocean acidification. *Limnology and Oceanography*, *55*(1), 346–353. https://doi.org/10.4319/lo.2010.55.1.0346

Boyer, T. P., Baranova, O. K., Coleman, C., Garcia, H. E., Grodsky, A., Locarnini, R. A., et al. (2018). *World Ocean Database 2018: Chapter 1. Introduction*. NOAA Atlas NESDIS NCEI, Silver Spring. Retrieved from https://data.nodc.noaa.gov/woa/WOD/DOC/wod_intro.pdf

Brodeur, J. R., Chen, B., Su, J., Xu, Y., Hussain, N., Scaboo, K. M., et al. (2019). Chesapeake Bay inorganic carbon: Spatial distribution and seasonal variability. *Frontiers in Marine Science*, *6*(99). https://doi.org/10.3389/fmars.2019.00099

Cai, W., Feely, R. A., Testa, J. M., Li, M., Evans, W., Alin, S. R., et al. (2020). Natural and anthropogenic drivers of acidification in large estuaries. *Annual Review of Marine Science*, *13*, 1. https://doi.org/10.1146/annurev-marine-010419-011004

Cai, W., Hu, X., Huang, W., Jiang, L., Wang, Y., Peng, T., & Zhang, X. (2010). Alkalinity distribution in the western North Atlantic Ocean margins. *Journal of Geophysical Research: Oceans*, *115*, C08014. https://doi.org/10.1029/2009JC005482

Cai, W., Hu, X., Huang, W., Murrell, M. C., Lehrter, J. C., Lohrenz, S. E., et al. (2011). Acidification of subsurface coastal waters enhanced by eutrophication. *Nature Geoscience*, *4*(11), 766–770. https://doi.org/10.1038/ngeo1297

Cai, W., Huang, W., Luther, G. W., Pierrot, D., Li, M., Testa, J. M., et al. (2017). Redox reactions and weak buffering capacity lead to acidification in the Chesapeake Bay. *Nature Communications*, *8*, 369. https://doi.org/10.1038/s41467-017-00417-7

Cai, W., & Wang, Y. (1998). The chemistry, fluxes, and sources of carbon dioxide in the estuarine waters of the Satilla and Altamaha Rivers, Georgia. *Limnology and Oceanography*, *43*(4), 657–668. https://doi.org/10.4319/lo.1998.43.4.0657

Cai, W., Xu, Y., Feely, R. A., Wanninkhof, R., Jönsson, B., Alin, S. R., et al. (2020). Controls on surface water carbonate chemistry along North American ocean margins. *Nature Communications*, *11*, 2691. https://doi.org/10.1038/s41467-020-16530-z

Carstensen, J., & Duarte, C. M. (2019). Drivers of pH variability in coastal ecosystems. *Environmental Science & Technology*, *53*, 4020–4029. https://doi.org/10.1021/acs.est.8b03655

Chen, B., Cai, W., Brodeur, J. R., Hussain, N., Testa, J. M., Ni, W., & Li, Q. (2020). Seasonal and spatial variability in surface pCO_2 and air–water CO_2 flux in the Chesapeake Bay. *Limnology and Oceanography*, *65*, 3046–3065. https://doi.org/10.1002/lno.11573

Chesapeake Bay National Estuarine Research Reserve in Virginia, Virginia Institute of Marine Science (CBNERR-VA VIMS) (2020). *Virginia Estuarine and Coastal Observing System (VECOS)*. Data accessed from VECOS website: accessed on 06 May 2020. Retrieved from http://vecos.vims.edu

Chesapeake Bay Program. (2012). *Guide to using Chesapeake Bay program water quality monitoring data*. Retrieved from https://www.chesapeakebay.net/documents/3676/wq_data_userguide_10feb12_mod.pdf

Chesapeake Bay Program. (2017). *Online draft documentation for Phase 6 modeling tools. Chesapeake Bay program Office*. Annapolis. Retrieved from https://www.chesapeakebay.net/documents/Phase_6_Modeling_Tools_1-page_factsheet_12-18-17.pdf

Copernicus Climate Change Service (C3S). (2017). ERA5: Fifth generation of ECMWF atmospheric reanalyzes of the global climate. Copernicus Climate Change Service Climate Data Store (CDS), date of access. Retrieved from https://cds.climate.copernicus.eu/cdsapp#!/home

Da, F., Friedrichs, M. A. M., & St-Laurent, P. (2018). Impacts of atmospheric nitrogen deposition and coastal nitrogen fluxes on Chesapeake Bay hypoxia. *Journal of Geophysical Research: Oceans*, *123*(7), 5004–5025. https://doi.org/10.1029/2018JC014009

Dickson, A. G., Sabine, C. L., & Christian, J. R.(Eds.) (2007).*Guide to best practices for ocean CO_2 measurement*. PICES Special Publication 3.

Dinauer, A., & Mucci, A. (2017). Spatial variability in surface-water pCO_2 and gas exchange in the world's largest semi-enclosed estuarine system: St. Lawrence estuary (Canada). *Biogeosciences*, *14*(13), 3221–3237. https://doi.org/10.5194/bg-14-3221-2017

Ding, H., & Elmore, A. J. (2015). Spatio-Temporal patterns in water surface temperature from Landsat time series data in the Chesapeake Bay, U.S.A. *Remote Sensing of Environment*, *168*, 335–348. https://doi.org/10.1016/j.rse.2015.07.009

Doney, S. C., Busch, D. S., Cooley, S. R., & Kroeker, K. J. (2020). The impacts of ocean acidification on marine ecosystems and reliant human communities. *Annual Review of Environment and Resources*, *45*, 83–112. https://doi.org/10.1146/annurev-environ-012320-083019

Doney, S. C., Fabry, V. J., Feely, R. A., & Kleypas, J. A. (2009). Ocean acidification: The other CO_2 problem. *Annual review of marine science*, *1*, 212–192. https://doi.org/10.1146/annurev.marine.010908.163834

Ekstrom, J. A., Suatoni, L., Cooley, S. R., Pendleton, L. H., Waldbusser, G. G., Cinner, J. E., et al. (2015). Vulnerability and adaptation of US shellfisheries to ocean acidification. *Nature Climate Change*, *5*, 207–214. https://doi.org/10.1038/nclimate2508

Feely, R. A., Alin, S. R., Newton, J., Sabine, C. L., Warner, M., Devol, A., et al. (2010). The combined effects of ocean acidification, mixing, and respiration on pH and carbonate saturation in an urbanized estuary. *Estuarine, Coastal and Shelf Science*, *88*(4), 442–449. https://doi.org/10.1016/j.ecss.2010.05.004

Feng, Y., Friedrichs, M. A. M., Wilkin, J., Tian, H., Yang, Q., Hofmann, E. E., et al. (2015). Chesapeake Bay nitrogen fluxes derived from a land-estuarine ocean biogeochemical modeling system: Model description, evaluation, and nitrogen budgets. *Journal of Geophysical Research: Biogeosciences*, *120*(8), 1666–1695. https://doi.org/10.1002/2015JG002931

Friedman, J. R., Shadwick, E. H., Friedrichs, M. A. M., Najjar, R. G., DeMeo, O. A., Da, F., & Smith, J. (2020). Seasonal variability of the CO_2 system in a large coastal plain estuary. *Journal of Geophysical Research: Oceans*, *125*(1). https://doi.org/10.1029/2019JC015609

Garcia, H. E., & Gordon, L. L. (1992). Oxygen solubility in seawater: Better fitting equations. *Limnology and Oceanography*, *37*(6), 1307–1312. https://doi.org/10.4319/lo.1992.37.6.1307

Gobler, C. J., & Baumann, H. (2016). Hypoxia and acidification in ocean ecosystems: Coupled dynamics and effects on marine life. *Biology Letters*, *12*(5), 20150976. https://doi.org/10.1098/rsbl.2015.0976

Gobler, C. J., DePasquale, E. L., Griffith, A. W., & Baumann, H. (2014). Hypoxia and acidification have additive and synergistic negative effects on the growth, survival, and metamorphosis of early life stage bivalves. *PloS ONE*, *9*(1), e83648. https://doi.org/10.1371/journal.pone.0083648

Gobler, C. J., & Talmage, S. C. (2013). Short and long-term consequences of larval stage exposure to constantly and ephemerally elevated carbon dioxide for marine bivalve populations. *Biogeosciences*, *10*, 2241–2253. https://doi.org/10.5194/bg-10-2241-2013

Goldsmith, K. A., Lau, S., Poach, M. E., Sakowicz, G. P., Trice, T. M., Ono, R. C., et al. (2019). Scientific considerations for acidification monitoring in the U.S. Mid-Atlantic region. *Estuarine, Coastal and Shelf Science*, *225*, 106189. https://doi.org/10.1016/j.ecss.2019.04.023

Hagy, J. D., Boynton, W. R., Keefe, C. W., & Wood, K. V. (2004). Hypoxia in Chesapeake Bay, 1950-2001: Long-term change in relation to nutrient loading and river flow. *Estuaries and Coasts*, *27*(4), 634–658. https://doi.org/10.1007/BF02907650

Harding, L. W., Gallegos, C. L., Perry, E. S., Miller, W. D., Adolf, J. E., Mallonee, M. E., & Paerl, H. W. (2016). Long-term trends of nutrients and phytoplankton in Chesapeake Bay. *Estuaries and Coasts*, *39*, 664–681. https://doi.org/10.1007/s12237-015-0023-7

Harding, L. W., Mallonee, M. E., & Perry, E. S. (2002). Toward a predictive understanding of primary productivity in a temperate, partially stratified estuary. *Estuarine, Coastal and Shelf Science*, *55*(3), 437–463. https://doi.org/10.1006/ecss.2001.0917

Hartmann, D. L., Klein Tank, A. M. G., Rusticucci, M., Alexander, L. V., Brönnimann, S., Charabi, Y. A. R., et al. (2013). IPCC, Climate Change 2013: The Physical Science Basis. Contribution of Working Group I to the Fifth Assessment Report of the Intergovernmental Panel on Climate Change (pp. 187–194). https://doi.org/10.1017/CBO9781107415324.008

Herrmann, M., Najjar, R. G., Da, F., Friedman, J. R., Friedrichs, M. A. M., Goldberger, S., et al. (2020). Challenges in quantifying air-water carbon dioxide flux using estuarine water quality data: Case study for Chesapeake Bay. *Journal of Geophysical Research: Oceans*, *125*, e2019JC015610. https://doi.org/10.1029/2019JC015610

Hinson, K., Friedrichs, M. A. M., St-Laurent, P., Da, F., & Najjar, R. G. (2021). Extent and causes of Chesapeake Bay warming. *Journal of the American Water Resources Association*. 1–21. https://doi.org/10.1111/1752-1688.12916

Hofmann, E., Druon, J., Fennel, K., Friedrichs, M. A. M., Haidvogel, D., Lee, C., et al. (2008). Eastern U.S. continental shelf carbon budget integrating models, data assimilation, and analysis. *Oceanography*, *21*(1), 86–104. https://doi.org/10.5670/oceanog.2008.70

Hopkinson, C. S., Buffam, I., Hobbie, J., Vallino, J., Perdue, M., Eversmeyer, B., et al. (1998). Terrestrial inputs of organic matter to coastal ecosystems: An intercomparison of chemical characteristics and bioavailability. *Biogeochemistry*, *43*, 211–234. https://doi.org/10.1023/A:1006016030299

Hudson, K., & Virginia Sea Grant marine advisory Program (2019). Virginia Shellfish Aquaculture Situation and Outlook Report: Results of the 2018 Virginia Shellfish Aquaculture Crop Reporting Survey.Marine resource report No. 2019-8; Virginia Sea Grant VSG-19-03. Virginia Institute of Marine Science, William & Mary. https://doi.org/10.25773/jc19-y847

Irby, I. D., & Friedrichs, M. A. M. (2019). Evaluating confidence in the impact of regulatory nutrient reduction on Chesapeake Bay water quality. *Estuaries and Coasts*, *42*, 16–32. https://doi.org/10.1007/s12237-018-0440-5

Irby, I. D., Friedrichs, M. A. M., Da, F., & Hinson, K. E. (2018). The competing impacts of climate change and nutrient reductions on dissolved oxygen in Chesapeake Bay. *Biogeosciences*, *15*, 2649–2668. https://doi.org/10.5194/bg-2017-41610.5194/bg-15-2649-2018

Johnson, G. C., & Lyman, J. M. (2020). Warming trends increasingly dominate global ocean. *Nature Climate Change*, *10*, 757–761. https://doi.org/10.1038/s41558-020-0822-0

Jolliff, J. K., Kindle, J. C., Shulman, I., Penta, B., Friedrichs, M. A. M., Helber, R., & Arnone, R. A. (2009). Summary diagrams for coupled hydrodynamic-ecosystem model skill assessment. *Journal of Marine Systems*, *76*(1–2), 64–82. https://doi.org/10.1016/j.jmarsys.2008.05.014

Kaushal, S. S., Likens, G. E., Utz, R. M., Pace, M. L., Grese, M., & Yepsen, M. (2013). Increased river alkalinization in the Eastern U.S. *Environmental Science & Technology*, *47*(18), 10302–10311. https://doi.org/10.1021/es401046s

Keeling, R. F., & Keeling, C. D. (2017). Atmospheric monthly in situ CO_2 data—Mauna Loa Observatory, Hawaii. In *Scripps CO_2 program data*. UC San Diego Library Digital Collections. https://doi.org/10.6075/J08W3BHW. Accessed on September 11, 2020.

Kemp, W. M., Boynton, W. R., Adolf, J. E., Boesch, D. F., Boicourt, W. C., Brush, G., et al. (2005). Eutrophication of Chesapeake Bay: Historical trends and ecological interactions. *Marine Ecology Progress Series*, *303*, 1–29. https://doi.org/10.3354/meps303001

Kemp, W. M., Smith, E. M., Marvin-DiPasquale, M., & Boynton, & W. R. (1997). Organic carbon balance and net ecosystem metabolism in Chesapeake Bay. *Marine Ecology Progress Series*, *150*, 229–248. https://doi.org/10.3354/meps150229

Kim, G. E., St-Laurent, P., Friedrichs, M. A. M., & Mannino, A. (2020). Impacts of water clarity variability on temperature and biogeochemistry in the Chesapeake Bay. *Estuaries and Coasts*, *43*, 1973–1991. https://doi.org/10.1007/s12237-020-00760-x

Lefcheck, J. S., Orth, R. J., Dennison, W. C., Wilcox, D. J., Murphy, R. R., Keisman, J., et al. (2018). Long-term nutrient reductions lead to the unprecedented recovery of a temperate coastal region. *Proceedings of the National Academy of Sciences of the United States of America*, *115*(14), 3658–3662. https://doi.org/10.1073/pnas.1715798115

Lomas, M. W., Gilbert, P. M., Shiah, F. K., & Smith, E. M. (2002). Microbial processes and temperature in Chesapeake Bay: Current relationships and potential impacts of regional warming. *Global Change Biology*, *8*(1), 51–70. https://doi.org/10.1046/j.1365-2486.2002.00454.x

Mesinger, F., DiMego, G., Kalnay, E., Mitchell, K., Shafran, P. C., Ebisuzaki, W., et al. (2006). North American Regional Reanalysis: A long-term, consistent, high-resolution climate dataset for the North American domain, as a major improvement upon the earlier global reanalysis datasets in both resolution and accuracy. *Bulletin of the American Meteorological Society*, *87*, 343–360. https://doi.org/10.1175/BAMS-87-3-343

Moriarty, J. M., Friedrichs, M. A. M., & Harris, C. K. (2021). Seabed resuspension in the Chesapeake Bay: Implications for biogeochemical cycling and hypoxia. *Estuaries and Coasts*, *44*, 103–122. https://doi.org/10.1007/s12237-020-00763-8

Moyer, D. L., & Blomquist, J. D. (2020).*Nitrogen, phosphorus, and suspended-sediment loads and trends measured at the Chesapeake Bay River Input Monitoring stations—Water years 1985–2019*. U. S. Geological Survey data release. https://doi.org/10.5066/P9VG459V

Muhling, B. A., Gaitán, C. F., Stock, C. A., Vincent, S. S., Tommasi, D., & Dixon, K. W. (2018). Potential salinity and temperature futures for the Chesapeake Bay using a statistical Downscaling Spatial Disaggregation Framework. *Estuaries and Coasts*, *41*, 349–372. https://doi.org/10.1007/s12237-017-0280-8

Najjar, R. G., Herrmann, M., Cintrón Del Valle, S., Friedman, J. R., Friedrichs, M. A. M., Harris, L. A., et al. (2020). Alkalinity in tidal tributaries of the Chesapeake Bay. *Journal of Geophysical Research: Oceans*, *125*, e2019JC015597. https://doi.org/10.1029/2019JC015597

Ni, W., Li, M., & Testa, J. M. (2020). Discerning effects of warming, sea level rise and nutrient management on long-term hypoxia trends in Chesapeake Bay. *The Science of the Total Environment*, *737*, 139717. https://doi.org/10.1016/j.scitotenv.2020.139717

Nixon, S. W. (1995). Coastal marine eutrophication: A definition, social causes, and future concerns. *Ophelia*, *41*, 199–219. https://doi.org/10.1080/00785236.1995.10422044

Olson, M., Malonee, M., & Ley, M. E. (2012). Guide to Using Chesapeake Bay Program Water Quality Monitoring Data, (February). (Vol. 159).EPA 908-R-12-001.

Osborne, E. B., Thunell, R. C., Gruber, N., Feely, R. A., & Benitez-Nelson, C. R. (2020). Decadal variability in twentieth-century ocean acidification in the California Current Ecosystem. *Nature Geoscience*, *13*, 43–49. https://doi.org/10.1038/s41561-019-0499-z

Pan, S., Bian, Z., Tian, H., Yao, Y., Najjar, R. G., Friedrichs, M. A. M., et al. (2021). Impacts of multiple environmental changes on long–term nitrogen loading from the Chesapeake Bay watershed. *Journal of Geophysical Research: Biogeosciences*, *126*. https://doi.org/10.1029/2020JG005826

Raymond, P. A., & Hamilton, S. K. (2018). Anthropogenic influences on riverine fluxes of dissolved inorganic carbon to the oceans. *Limnology and Oceanography Letters*, *3*(3), 143–155. https://doi.org/10.1002/lol2.10069

Raymond, P. A., & Oh, N.-H. (2009). Long term changes of chemical weathering products in rivers heavily impacted from acid mine drainage: Insights on the impact of coal mining on regional and global carbon and sulfur budgets. *Earth and Planetary Science Letters*, *28*(1–2), 50–56. https://doi.org/10.1016/j.epsl.2009.04.006

Rheuban, J. E., Doney, S. C., McCorkle, D. C., & Jakuba, R. W. (2019). Quantifying the effects of nutrient enrichment and freshwater mixing on coastal ocean acidification. *Journal of Geophysical Research: Oceans*, *124*, 9085–9100. https://doi.org/10.1029/2019JC015556

Saba, V. S., Griffies, S. M., Anderson, W. G., Winton, M., AlexanderDelworth, M. A. T. L., Delworth, T. L., et al. (2016). Enhanced-warming of the Northwest AtlanticOcean under climate change. *Journal of Geophysical Research: Oceans*, *121*, 118–132. https://doi.org/10.1002/2015JC011346

Salisbury, J. E., & Jönsson, B. F. (2018). Rapid warming and salinity changes in the Gulf of Maine alter surface ocean carbonate parameters and hide ocean acidification. *Biogeochemistry*, *141*, 401–418. https://doi.org/10.1007/s10533-018-0505-3

Seliger, H. H., Boggs, J. A., & Biggley, W. H. (1985). Catastrophic anoxia in the Chesapeake Bay in 1984. *Science*, *228*(4695), 70–73. https://doi.org/10.1126/science.228.4695.70

Shadwick, E. H., De Meo, O. A., & Friedman, J. R. (2019). *Discrete CO_2–system measurements in the Chesapeake Bay mainstem between 2016 and 2018*. Data, William & Mary. https://doi.org/10.25773/rntn-ez18

Shadwick, E. H., Friedrichs, M. A. M., Najjar, R. G., DeMeo, O. A., Friedman, J. R., Da, F., & Reay, W. G. (2019). High-frequency CO_2-system variability over the winter-to-spring transition in a coastal plain estuary. *Journal of Geophysical Research: Oceans*, *124*(11), 7626–7642. https://doi.org/10.1029/2019JC015246

Shchepetkin, A., & McWilliams, J. (2005). The regional ocean modeling system (ROMS): A split-explicit, free-surface, topography-following-coordinate ocean model. *Ocean Modelling*, *9*, 347–404. https://doi.org/10.1016/j.ocemod.2004.08.002

Shen, C., Testa, J. M., Li, M., & Cai, W. (2020). Understanding anthropogenic impacts on pH and aragonite saturation state in Chesapeake Bay: Insights from a 30-year model study. *Journal of Geophysical Research: Biogeosciences*, *125*, e2019JG005620. https://doi.org/10.1029/2019JG005620

Shen, C., Testa, J. M., Li, M., Cai, W., Waldbusser, G. G., Ni, W., et al. (2019). Controls on carbonate system dynamics in a coastal plain estuary: A modeling study. *Journal of Geophysical Research: Biogeosciences*, *124*, 61–78. https://doi.org/10.1029/2018JG004802

Son, S., Wang, M., & Harding, L. W. (2014). Satellite-measured net primary production in the Chesapeake Bay. *Remote Sensing of Environment*, *144*, 109–119. https://doi.org/10.1016/j.rse.2014.01.018

St-Laurent, P., Friedrichs, M. A. M., Najjar, R. G., Shadwick, E. H., Tian, H., & Yao, Y. (2020). Relative impacts of global changes and regional watershed changes on the inorganic carbon balance of the Chesapeake Bay. *Biogeosciences*, *17*(14), 3779–3796. https://doi.org/10.5194/bg-17-3779-2020

Stets, E. G., Kelly, V. J., & Crawford, C. G. (2014). Long-term trends in alkalinity in large rivers of the conterminous US in relation to acidification, agriculture, and hydrologic modification. *Science of the Total Environment*, *488–489*, 280–289. https://doi.org/10.1016/j.scitotenv.2014.04.054

Su, J., Cai, W., Brodeur, J., Chen, B., Hussain, N., Yao, Y., et al. (2020). Chesapeake Bay acidification buffered by spatially decoupled carbonate mineral cycling. *Nature Geoscience*, *13*, 441–447. https://doi.org/10.1038/s41561-020-0584-3

Sunda, W. G., & Cai, W. (2012). Eutrophication induced CO_2-acidification of subsurface coastal waters: Interactive effects of temperature, salinity, and atmospheric pCO_2. *Environmental Science & Technology*, *46*(19), 10651–10659. https://doi.org/10.1021/es300626f

Sutton, A., & Newton, J. A. (2020). Reaching consensus on assessments of ocean acidification trends. *Eos*, *101*. https://doi.org/10.1029/2020EO150944

Sydeman, W. J., Garcia-Reyes, M., Schoeman, D. S., Rykaczewski, R. R., Thompson, S. A., Black, B. A., & Bograd, S. J. (2014). Climate change and wind intensification in coastal upwelling ecosystems. *Science*, *345*(6192), 77–80. https://doi.org/10.1126/science.1251635

Takahashi, T., Sutherland, S. C., Chipman, D. W., Goddard, J. G., Ho, C., Newberger, T., et al. (2014). Climatological distributions of pH, pCO_2, total CO_2, alkalinity, and $CaCO_3$ saturation in the global surface ocean, and temporal changes at selected locations. *Marine Chemistry*, *164*, 95–125. https://doi.org/10.1016/j.marchem.2014.06.004

Talmage, S. C., & Gobler, C. J. (2011). Effects of elevated temperature and carbon dioxide on the growth and survival of larvae and juveniles of three species of Northwest Atlantic bivalves. *PloS One*, *6*(10), e26941. https://doi.org/10.1371/journal.pone.0026941

Tomasetti, S. J., & Gobler, C. J. (2020). Dissolved oxygen and pH criteria leave fisheries at risk. *Science*, *368*(6489), 372–373. https://doi.org/10.1126/science.aba4896

Turner, J. S., St-Laurent, P., Friedrichs, M. A. M., & Friedrichs, C. T. (2021). Effects of reduced shoreline erosion on Chesapeake Bay water clarity. *Science of the Total Environment*, *769*, 14517. https://doi.org/10.1016/j.scitotenv.2021.145157

USEPA (U.S. Environmental Protection Agency). (2010). *Chesapeake Bay total maximum daily load for nitrogen, phosphorus, and sediment*, US Environmental Protection Agency, US Environmental Protection Agency Chesapeake Bay Program Office.

VanDam, B. R., & Wang, H. (2019). Decadal-scale acidification trends in adjacent North Carolina estuaries: Competing role of anthropogenic CO_2 and riverine alkalinity loads. *Frontiers in Marine Science*, *6*, 136. https://doi.org/10.3389/fmars.2019.00136

vanHeuven, S., Pierrot, D., Rae, J. W. B., Lewis, E., & Wallace, D. W. (2011). Matlab program developed for CO2 system calculations (Tech. Rep.): ORNL/CDIAC.

Waldbusser, G. G., Brunner, E. L., Haley, B. A., Hales, B., Langdon, C. J., & Prahl, F. G. (2013). A developmental and energetic basis linking larval oyster shell formation to acidification sensitivity. *Geophysical Research Letters*, *40*, 2171–2176. https://doi.org/10.1002/grl.50449

Waldbusser, G. G., Hales, B., Langdon, C., Haley, B. A., Schrader, P., Brunner, E. L., et al. (2015). Saturation-state sensitivity of marine bivalve larvae to ocean acidification. *Nature Climate Change*, *5*, 273–280. https://doi.org/10.1038/nclimate2479

Waldbusser, G. G., & Salisbury, J. E. (2014). Ocean acidification in the coastal zone from an organism's perspective: Multiple system parameters, frequency domains, and habitats. *Annual Reviews of Marine Science*, *6*, 221–247. https://doi.org/10.1146/annurev-marine-121211-172238

Waldbusser, G. G., Voigt, E. P., Bergschneider, H., Green, M., & Newell, R. I. E. (2011). Biocalcification in the Eastern Oyster (*Crassostrea virginica*) in relation to long-term trends in Chesapeake Bay pH. *Estuaries and Coasts*, *4*, 221–231. https://doi.org/10.1007/s12237-010-9307-0

Wanninkhof, R. (1992). Relationship between gas exchange and wind speed over the ocean. *Journal of Geophysical Research: Oceans*, *97*, 7373–7381. https://doi.org/10.1029/92jc00188

Wanninkhof, R. (2014). Relationship between wind speed and gas exchange over the ocean revisited. *Limnology and Oceanography: Methods*, *12*, 351–362. https://doi.org/10.4319/lom.2014.12.351

Wolf-Gladrow, D. A., Zeebe, R. E., Klaas, C., Körtzingera, A., & Dickson, A. G. (2007). Total alkalinity: The explicit conservative expression and its application to biogeochemical processes. *Marine Chemistry*, *106*(1–2), 287–300. https://doi.org/10.1016/j.marchem.2007.01.006

Xu, J., Long, W., Wiggert, J. D., Lanerolle, L. W. J., Brown, C. W., Murtugudde, R., & Hood, R. R. (2012). Climate forcing and salinity variability in Chesapeake Bay, USA. *Estuarine Coastal and Shelf Science*, *35*(1), 237–261. https://doi.org/10.1007/s12237-011-9423-5

Xu, Y., Cai, W., Wanninkhof, R., Salisbury, J. E., Reimer, J., & Chen, B. (2020). Long-term changes of carbonate chemistry variables along the North American East Coast. *Journal of Geophysical Research: Oceans*, *125*, e2019JC015982. https://doi.org/10.1029/2019JC015982

Yang, Q., Tian, H., Friedrichs, M. A. M., Hopkinson, C. S., Lu, C., & Najjar, R. G. (2015). Increased nitrogen export from eastern North America to the Atlantic Ocean due to climatic and anthropogenic changes during 1901–2008. *Journal of Geophysical Research: Biogeosciences*, *120*, 1046–1068. https://doi.org/10.1002/2014JG002763

Zhang, Q., & Blomquist, J. D. (2018). Watershed export of fine sediment, organic carbon, and chlorophyll-a to Chesapeake Bay: Spatial and temporal patterns in 1984–2016. *The Science of the Total Environment*, *619–620*, 1066–1078. https://doi.org/10.1016/j.scitotenv.2017.10.279

Zhang, Q., Brady, D. C., Boynton, W. R., & Ball, W. P. (2015). Long-Term trends of nutrients and sediment from the nontidal Chesapeake Watershed: An assessment of progress by river and season. *Journal of the American Water Resources Association*, *51*(6), 1534–1555. https://doi.org/10.1111/1752-1688.12327

Zhao, Y., Liu, J., Uthaipan, K., Song, X., Xu, Y., He, B., et al. (2020). Dynamics of inorganic carbon and pH in a large subtropical continental shelf system: Interaction between eutrophication, hypoxia, and ocean acidification. *Limnology and Oceanography*, *65*(6), 1359–1379. https://doi.org/10.1002/lno.11393